ANNUAL REVIEWS

Annual Review of Chemical and Biomolecular Engineering

Numerical Methods for the Solution of Population Balance Equations Coupled with Computational Fluid Dynamics

Mohsen Shiea, Antonio Buffo, Marco Vanni, and Daniele Marchisio

Department of Applied Science and Technology, Institute of Chemical Engineering, Politecnico di Torino, 10129 Torino, Italy; email: daniele.marchisio@polito.it

Annu. Rev. Chem. Biomol. Eng. 2020. 11:339–66

First published as a Review in Advance on April 6, 2020

The *Annual Review of Chemical and Biomolecular Engineering* is online at chembioeng.annualreviews.org

https://doi.org/10.1146/annurev-chembioeng-092319-075814

Keywords

population balance equation, computational fluid dynamics, multiphase flow, crystallization, gas–liquid systems, liquid–liquid systems, quadrature-based moment methods

Abstract

This review article discusses the solution of population balance equations, for the simulation of disperse multiphase systems, tightly coupled with computational fluid dynamics. Although several methods are discussed, the focus is on quadrature-based moment methods (QBMMs) with particular attention to the quadrature method of moments, the conditional quadrature method of moments, and the direct quadrature method of moments. The relationship between the population balance equation, in its generalized form, and the Euler-Euler multiphase flow models, notably the two-fluid model, is thoroughly discussed. Then the closure problem and the use of Gaussian quadratures to overcome it are analyzed. The review concludes with the presentation of numerical issues and guidelines for users of these modeling approaches.

1. INTRODUCTION

Computational fluid dynamics (CFD) for simulation of disperse multiphase systems has gained considerable importance in the last two decades because of its widespread application in chemical, biochemical, pharmaceutical, and aerospace industries. Disperse multiphase systems are formed by separate entities, i.e., particles/crystals, drops, and bubbles, being dispersed in a continuous phase. The characteristic properties of the disperse phase elements change in space and time due to numerous particulate processes, such as collisions, aggregation/coalescence, breakage, nucleation, dissolution/evaporation, and mass and heat transfer. As a result, disperse systems often feature distributions of elements with different properties, a situation identified as polydispersity. A comprehensive simulation of disperse systems must take into account polydispersity and therefore must include the description of the above-mentioned processes. The most common computational approaches employed in this field can be categorized in three main groups: fully resolved interface-tracking models, Lagrangian point-particle models, and Eulerian-Eulerian models. This review focuses on the last group of methods, which has a simpler level of detail than the other two groups but is suitable for CFD simulation of multiphase systems, particularly those of industrial scale.

Eulerian-Eulerian methods in their original formulation (in the 1990s) required the specification of the mean size of disperse phase elements. Setting this number fixed and constant, it was simply impossible to account for polydispersity and for the effect of particulate processes. It was only in the 2000s that their coupling with population balance equations (PBEs) was realized and the relationship between PBEs and Eulerian-Eulerian models was investigated and clarified. This review reports a critical discussion of these issues. In particular, it explains how the solution of the PBE provides a detailed level of description of the disperse phase, which is not accessible from CFD models alone, leading to a more accurate simulation of the entire system. To this purpose, a suitable method for the solution of the PBE should be selected, considering several factors such as the nature of the system under study, the required level of description, and the available computational resources. The current review covers several methods for the solution of the PBE, which belong to three main categories: the class or sectional method (CM), the method of moments (MOM), and the quadrature-based moment methods (QBMMs). Further, a separate section addresses the implementation of PBEs in CFD and discusses some numerical issues concerning the stability of simulations. The review concludes by discussing the most popular implementations in commercial and open-source CFD-PBE codes.

2. GOVERNING EQUATIONS

2.1. Population Balance Equation

The PBE is a continuity statement that governs the evolution of a number density function (NDF), which is postulated to exist for a population of disperse phase elements. The NDF defines the distribution of the disperse phase elements over the properties of interest at any time instant and physical position. These properties, called internal coordinates, characterize the disperse elements and can include velocity, size, composition, temperature, etc. The choice of the internal coordinates, denoted here by the vector $\boldsymbol{\xi}$, is system dependent. The state of a generic element q at time t can be determined by its position vector $\mathbf{x}^{(q)}$ and internal coordinates $\boldsymbol{\xi}^{(q)}$, jointly called the element state vector $(\mathbf{x}^{(q)}, \boldsymbol{\xi}^{(q)})$. The state vector of a given element specifies the location of that element in the so-called phase-space, which is a high-dimensional space consisting of the physical domain of the system $\Omega_{\mathbf{x}}$ and the domain of the internal coordinates $\Omega_{\boldsymbol{\xi}}$. Given an arbitrary point in the phase-space $(\mathbf{x}, \boldsymbol{\xi})$, the NDF $n(t, \mathbf{x}, \boldsymbol{\xi})$ is defined as the expected number density of elements in the infinitesimal volume $\mathrm{d}\mathbf{x}\,\mathrm{d}\boldsymbol{\xi}$ around that point at time t (1).

At first, let the velocity of the disperse phase elements be known and excluded from the internal coordinate vector. Then the PBE takes the following form (2):

$$\partial_t n + \partial_{\mathbf{x}} \cdot (\mathbf{U}_{\mathrm{d}} n) + \partial_{\boldsymbol{\xi}} \cdot (\mathbf{G} n) = \mathcal{S}, \qquad 1.$$

where $\mathbf{U}_{\mathrm{d}}(\boldsymbol{\xi})$ is the velocity of the disperse phase elements and $\mathbf{G}(\boldsymbol{\xi})$ is the rate of change of the internal coordinates due to continuous molecular processes, such as mass and heat transfer, growth and dissolution of elements, and chemical reactions. The source term $\mathcal{S}(\boldsymbol{\xi})$ describes the discontinuous changes in the internal coordinates of the elements due to discrete events, which are generally categorized as second-order, first-order, and zero-order point processes.

The mathematical form of $\mathcal{S}$ can be illustrated by the following example. If the only internal coordinate is the mass (or the volume) of the disperse phase elements that undergo aggregation/coalescence and breakage, then the source term becomes (space and time dependency is omitted for brevity) (1):

$$\begin{aligned}\mathcal{S}(\xi) = \frac{1}{2}\int_0^{\xi} a(\xi-\xi',\xi)\, n(\xi-\xi')\, n(\xi)\, \mathrm{d}\xi' - n(\xi)\int_0^{\infty} a(\xi,\xi')\, n(\xi')\, \mathrm{d}\xi' \\ + \int_{\xi}^{\infty} b(\xi')\, \beta(\xi|\xi')\, n(\xi')\, \mathrm{d}\xi' - b(\xi)\, n(\xi), \qquad 2.\end{aligned}$$

where $a(\xi, \xi')$ denotes the rate of aggregation/coalescence between pairs of elements whose internal coordinates are equal to ξ and ξ' (i.e., aggregation kernel) and $b(\xi)$ is the rate of breakage of elements whose internal coordinate is equal to ξ (i.e., breakage kernel). In addition, $\beta(\xi|\xi')$ is the so-called daughter distribution and statistically defines the number of daughter elements whose internal coordinate is equal to ξ, formed due to the breakage of an element whose internal coordinate is ξ'. On the right-hand side of Equation 2, the first and third terms describe the birth of new elements due to coalescence and breakage, respectively, whereas the second and fourth terms take into account the death of elements due to coalescence and breakage, respectively.

Equation 1 is a high-dimensional transport (or kinetic) equation that describes the evolution of the NDF not only in time and physical space but also in the domain of internal coordinates. The velocity of the disperse phase in Equation 1 ($\mathbf{U}_{\mathrm{d}}$) is assumed to be a known function of time, spatial position, and internal coordinates ($\boldsymbol{\xi}$). In addition, the flow fields of the continuous phase, e.g., velocity ($\mathbf{U}_{\mathrm{c}}$), are generally required by the closure relations for the description of both continuous and discontinuous processes, i.e., $\mathbf{G}$ and $\mathcal{S}$. For this purpose, the velocity of both phases ($\mathbf{U}_{\mathrm{d}}$ and $\mathbf{U}_{\mathrm{c}}$) can be obtained by adopting an Eulerian CFD approach (see Section 2.3).

The velocity of the disperse phase elements ($\mathbf{u}$) must be included within the internal coordinate vector when different elements (with or without the same properties) located at the same position $\mathbf{x}$ and at the time instant t move with different velocities. In this case, the NDF $f(t, \mathbf{x}, \boldsymbol{\xi}, \mathbf{u})$ is defined as the expected number density of elements in the infinitesimal volume $\mathrm{d}\mathbf{x}\,\mathrm{d}\boldsymbol{\xi}\,\mathrm{d}\mathbf{u}$ around the arbitrary point $(\mathbf{x}, \boldsymbol{\xi}, \mathbf{u})$ at time t. The generalization of Equation 1 to include velocity as an internal coordinate leads to the following generalized population balance equation (GPBE) (2):

$$\partial_t f + \partial_{\mathbf{x}} \cdot (\mathbf{u} f) + \partial_{\boldsymbol{\xi}} \cdot (\mathbf{G} f) + \partial_{\mathbf{u}} \cdot (\mathbf{A} f) = \mathcal{S}. \qquad 3.$$

In Equation 3, $\mathbf{A}(\boldsymbol{\xi}, \mathbf{u})$ is the acceleration of the elements due to external forces, e.g., forces exerted from the continuous phase on the elements. The source term $\mathcal{S}(\boldsymbol{\xi}, \mathbf{u})$ is similar to that in the PBE except that it also describes the discontinuous change in the velocity of the elements due to discrete events (e.g., collisions).

First-order point process: a discrete event that involves a single disperse element, such as breakage

Second-order point process: a discrete event that involves two disperse elements, such as collision and aggregation/coalescence

Zero-order point process: a discrete event that does not involve any existing element, such as nucleation

Kinetic equation: number density function transport equation that includes the velocity of the elements as part of the internal coordinate vector

Stokes number: the ratio of the element relaxation time ($\tau_e = \frac{\rho_e d_e^2}{18\mu_c}$) to the characteristic time of the continuous phase (τ_c)

It is noteworthy that Equation 3 is closely related to Equation 1. In fact, as highlighted in some specific applications (3–8), the GPBE can be simplified by presuming a specific form for the NDF, $f(t, \mathbf{x}, \boldsymbol{\xi}, \mathbf{u}) = n(t, \mathbf{x}, \boldsymbol{\xi})\, \delta(\mathbf{u} - \langle \mathbf{u}|\boldsymbol{\xi}\rangle)$, which is called the monokinetic assumption. This is equivalent to assuming that the elements with the same internal coordinates move with the same velocity [i.e., the mean velocity conditioned on the internal coordinates $\langle \mathbf{u}|\boldsymbol{\xi}\rangle$ (3)]. Clearly this mean conditional velocity, defined as $\langle \mathbf{u}|\boldsymbol{\xi}\rangle = \int \mathbf{u} f \, \mathrm{d}\mathbf{u} \,/\, n(t, \mathbf{x}, \boldsymbol{\xi})$, is identical to $\mathbf{U}_\mathrm{d}(\boldsymbol{\xi})$, where $n(t, \mathbf{x}, \boldsymbol{\xi}) = \int f \, \mathrm{d}\mathbf{u}$ is the marginal NDF. The conditional velocity $\langle \mathbf{u}|\boldsymbol{\xi}\rangle$ can be calculated in different ways, by assuming for example a continuous parametric functional defined over the space of a chosen internal coordinate (2), or can be obtained by adopting Eulerian CFD models explained in Section 2.3.

2.2. Generalized Population Balance Equations in Turbulent Flow

In turbulent flows, in which turbulence is caused by instabilities in the continuous phase, the velocity of the continuous phase $\mathbf{U}_\mathrm{c}(t, \mathbf{x})$ is a random vector field characterized by fluctuations that result in fluctuations of the NDF defined previously. The direct solution of the GPBE/PBE, which resolves all the relevant length and time scales, is computationally expensive, and cheaper solutions are often sought. One alternative is to define a Reynolds-averaged NDF $\langle f \rangle(t, \mathbf{x}, \boldsymbol{\xi}, \mathbf{u})$ over an infinitely large number of realizations of the continuous phase velocity $\mathbf{U}_\mathrm{c}$ (2) and derive the following equation:

$$\partial_t \langle f \rangle + \partial_{\mathbf{x}} \cdot (\mathbf{u} \langle f \rangle) + \partial_{\boldsymbol{\xi}} \cdot (\langle \mathbf{G} f \rangle) + \partial_{\mathbf{u}} \cdot (\langle \mathbf{A} f \rangle) = \langle \mathcal{S} \rangle, \qquad 4.$$

leading to a Reynolds-averaged Navier-Stokes multiphase formulation. The terms $\langle \mathbf{G} f \rangle$, $\langle \mathbf{A} f \rangle$, and $\langle \mathcal{S} \rangle$ are generally not closed because the relations describing the continuous and discontinuous events depend on the continuous phase velocity, $\mathbf{U}_\mathrm{c}$. The above-mentioned terms are usually expressed as the summation of a mean field contribution and an additional contribution due to fluctuations, the latter of which needs a closure approximation. For example, Drew (9) used a kinetic equation describing the evolution of particles in turbulent flows to derive the Eulerian momentum balance equation, which includes a drag force due to the mean fields and an additional contribution, called turbulent dispersion force, due to turbulent fluctuations. It is noteworthy that spatial filtering (10) and large eddy simulation based on self-conditioned NDF (11) can be also used to derive the GPBE of the form of Equation 4.

2.3. Eulerian Computational Fluid Dynamics

This section describes three main Eulerian approaches for CFD simulation of multiphase flows. Generally, the applicability of CFD approaches depends on the multiphase properties, particularly those of the disperse phase. As shown in **Figure 1**, two key factors in selection of appropriate method are Stokes number and volume fraction of disperse phase elements. Another important factor is polydispersity index, as illustrated by **Figure 2**.

2.3.1. Dusty gas model. When disperse phase elements are sufficiently small, i.e., having a very small Stokes number, their trajectories are perfectly dictated by the velocity field of the continuous phase, $\mathbf{U}_\mathrm{c}$ (12). Thus, it is valid to assume that the elements move with a velocity equal to $\mathbf{U}_\mathrm{c}$. In such cases, the multiphase system is represented with one single continuous phase, whose properties, e.g., density and viscosity, are the same as the continuous phase for dilute systems, or otherwise are modified to consider the presence of disperse phase elements.

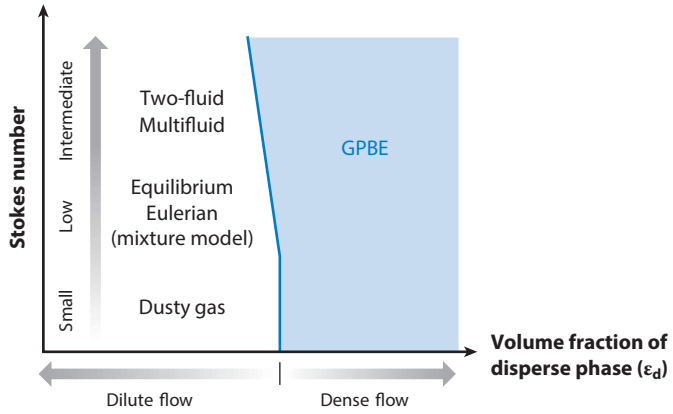

Figure 1

Applicability of the Eulerian computational fluid dynamics models for the simulation of multiphase flows. When the disperse elements' Stokes number is very small, the elements move with the same velocity of the continuous phase (dusty gas model). As the Stokes number increases, the elements' velocity may differ from that of the continuous phase due to their inertia, and it can be predicted by adopting mixture, two-fluid, or multifluid models. For the disperse elements with a large Stokes number, the equilibrium assumption of Eulerian–Eulerian methods is not generally valid, and adopting the generalized population balance equation (GPBE) is necessary to capture nonequilibrium phenomena. Last, in the case of dense flows, element–element interactions are significant and can be described by the GPBE.

2.3.2. Mixture model. As the Stokes number of elements increases, the elements move with a velocity that may differ from the one of the continuous phase. Under equilibrium assumption, the relative velocity between the disperse elements and the continuous phase can be expressed as an algebraic relation obtained from a force balance on the elements (usually drag and buoyancy forces). When the disperse system is dilute enough, one momentum balance equation is solved for the velocity of the continuous phase, and then the algebraic relation is used to calculate the velocity of the disperse phase. This model is referred to as the equilibrium Eulerian approach (13). Instead, when the number density of elements is higher, the disperse system is represented as one

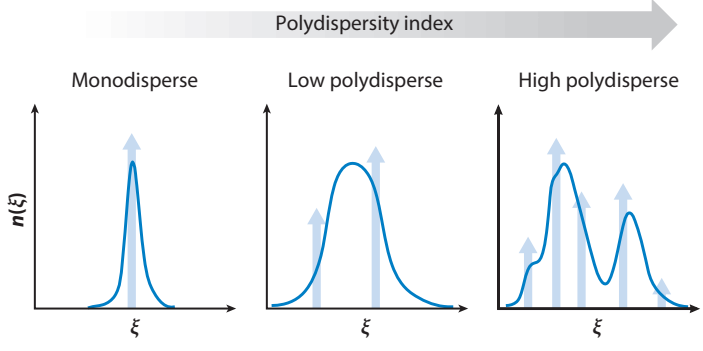

Figure 2

The polydispersity index indicates how widely the disperse phase elements are distributed over the space of the internal coordinate. The light blue arrows can be thought of as the nodes of the quadrature that approximates the underlying number density functions (*solid blue line*) or as the number of element groups required to consider the polydispersity appropriately.

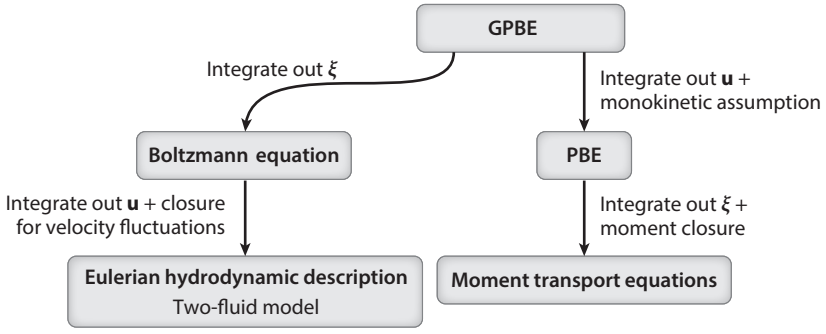

Figure 3

The relationship between the generalized population balance equation (GPBE), population balance equation (PBE), moments, and Eulerian computational fluid dynamics models.

mixture fluid, for which a momentum balance equation is solved. This balance equation requires the knowledge of the relative velocities, which are specified by using the algebraic relation. This approach is known as the mixture model (MM) (14, 15). An advantage of the MM is the possibility of taking into account the polydispersity of multiphase systems by dividing the disperse elements into groups based on an internal coordinate, e.g., size of elements. Then, the relative velocity between each group (fluid) and the continuous phase can be expressed separately, which eventually depends on the selected internal coordinate of elements.

2.3.3. Two- and multifluid models. The governing equations of the Eulerian two-fluid model (TFM) can be derived from the GPBE (see **Figure 3**). The derivation can be found elsewhere (2). For the sake of brevity, we report here only the mass and momentum balance equations for the continuous and disperse phases ($i = \mathrm{c}, \mathrm{d}$):

$$\partial_t(\rho_i \varepsilon_i) + \partial_{\mathbf{x}} \cdot (\rho_i \varepsilon_i \mathbf{U}_i) = 0, \qquad 5.$$

$$\partial_t(\rho_i \varepsilon_i \mathbf{U}_i) + \partial_{\mathbf{x}} \cdot (\rho_i \varepsilon_i \mathbf{U}_i \mathbf{U}_i) = \partial_{\mathbf{x}} \cdot (\varepsilon_i \boldsymbol{\tau}_i) - \varepsilon_i \partial_{\mathbf{x}} p + \rho_i \varepsilon_i \mathbf{g} + \mathbf{M}_i, \qquad 6.$$

where ρ_i, ε_i, and $\boldsymbol{\tau}_i$ denote the density, volume fraction, and stress tensor of the phase i, and p is the pressure (generally assumed the same for the continuous and disperse phases). The term $\mathbf{M}_i$ represents the momentum exchange between the continuous and disperse phases due to interfacial forces, such as drag and lift, and is generally modeled by closure relationships. For the disperse phase, the stress tensor $\boldsymbol{\tau}_i$ represents the dispersion of the element velocity ($\mathbf{u}$) around the mean disperse phase velocity ($\mathbf{U}_\mathrm{d}$). If the Stokes number of the elements is low enough, this stress tensor can be neglected; otherwise, it is necessary to solve transport equations for higher-order moments of the disperse element velocity (2). For the continuous phase, the stress tensor is modeled as for single-phase flows. When the flow is turbulent, the stress tensor of the continuous phase is generally closed by replacing the molecular viscosity with an effective one (16). The effective viscosity is the sum of the molecular viscosity and the turbulent viscosity, the latter of which is usually estimated by a two-equation model, e.g., the k–ε model, adapted for multiphase flows (17–20).

The TFM can be extended to consider more than two phases, e.g., dividing the disperse phase into several groups (fluids) based on the value of an internal coordinate (usually size). This approach, called the multifluid model (MFM), is particularly useful when the system under study is polydisperse (see **Figure 2**). The governing equations of the MFM have similar shapes to those of the TFM and can be found elsewhere (3, 4, 6, 7).

3. SOLUTION METHODS FOR POPULATION BALANCE EQUATIONS

Many methods are available in the literature for the numerical solution of PBEs; each has been developed to address the challenges posed by the application of interest. Some notable challenges include the number of internal coordinates, considering the element velocity as an internal coordinate (i.e., solving the GPBE), and the physical and chemical phenomena involved. This section describes three principal categories of methods for the solution of PBEs. Among the ones not covered in this review, we should cite Monte Carlo methods (1, 2), which are currently too computationally expensive to be compatible with CFD coupling.

3.1. Class or Sectional Method

The class or sectional method (CM) is based on the discretization of the internal coordinate space into intervals (classes or sections), such that the PBE is transformed into a set of macroscopic balance equations in the physical domain (1). This method has been widely applied to polydisperse systems governed by a univariate PBE. Let the space of the generic internal coordinate ξ be divided into M intervals using $M+1$ grid points $(\xi_1, \xi_2, \ldots, \xi_{M+1})$, therefore, the ith interval is defined as $I_i = [\xi_i, \xi_{i+1})$. The number density of elements in the interval I_i is given by $N_i(t, \mathbf{x}) = \int_{\xi_i}^{\xi_{i+1}} n(t, \mathbf{x}, \xi)\, \mathrm{d}\xi$, where $n(t, \mathbf{x}, \xi)$ is the NDF in Equation 1. Then, the discretized formulation of Equation 1 for the generic ith interval is

$$\partial_t N_i + \partial_{\mathbf{x}} \cdot (\mathbf{U}_i N_i) + \int_{\xi_i}^{\xi_{i+1}} \partial_\xi (Gn)\, \mathrm{d}\xi = \int_{\xi_i}^{\xi_{i+1}} \mathcal{S}\, \mathrm{d}\xi, \qquad 7.$$

where $\mathbf{U}_i$ is the velocity by which the elements of the ith interval are transported in the physical space. The integrals in Equation 7 are not closed, since they generally depend on the NDF and cannot be expressed in terms of N_i (1). A closed form of Equation 7 can be achieved by assuming a functional form for the NDF. Kumar & Ramkrishna (21) proposed a general procedure in which the NDF is approximated with the following form:

$$n(t, \mathbf{x}, \xi) = \sum_{i=1}^{M} N_i\, \delta(\xi - \zeta_i). \qquad 8.$$

The above approximation implies that all the elements belonging to the interval i are concentrated at a pivotal point ζ_i inside the interval. Another common approximation assumes a constant number density in each interval, i.e., $n(t, \mathbf{x}, \xi) = N_i$ for $\xi_i < \xi < \xi_{i+1}$ (22). In the following, we introduce the procedure proposed by Kumar & Ramkrishna (21) without going into full detail. For the sake of simplicity, the system is assumed to be homogeneous, i.e., the variables of interest (such as the NDF) have no dependency on the physical space. Moreover, the contribution due to the continuous changes is neglected at this stage and will be touched upon later.

In the case of aggregation and breakage, the right-hand side of Equation 7 can be written in the following closed form by assuming ξ to be a conserved property (1):

$$\int_{\xi_i}^{\xi_{i+1}} \mathcal{S}\, \mathrm{d}\xi = \frac{1}{2} \sum_{j=1}^{i-1} N_j \sum_{\substack{k \\ (\zeta_j + \zeta_k) \in I_i}} a(\zeta_j, \zeta_k) N_k - N_i \sum_{j=1}^{M} a(\zeta_i, \zeta_j) N_j$$

$$+ \sum_{j=i}^{M} b(\zeta_j) N_j \int_{\xi_i}^{\xi_{i+1}} \beta(\xi | \zeta_j)\, \mathrm{d}\xi - b(\xi_i) N_i. \qquad 9.$$

Kumar & Ramkrishna (21) explained in detail that the above formulation is not internally consistent, i.e., it does not generally preserve the integral properties of the NDF such as its moments. It is noteworthy that low-order moments of the NDF are associated with the conserved properties of the disperse phase. The cause of this internal inconsistency lies in the assignment of a pivotal point to the born elements, produced by the birth (first and third) terms in Equation 9. For instance, let two elements belonging to the intervals I_j and I_k with pivotal points ζ_j and ζ_k coalesce to form a new element i with $\xi_i = \zeta_j + \zeta_k$. Then, the value ξ_i determines which interval the element i belongs to. However, in an arbitrarily discretized space, ξ_i may not necessarily coincide with the pivotal point of the assigned interval. The same issue may arise when an element breaks into two daughter elements, which should be assigned to two intervals. Kumar & Ramkrishna (21) proposed to assign the born elements to the nearby pivotal points, such that two integral properties of the NDF are preserved. This approach, known as the fixed-pivot approach, is quite general and is internally consistent as far as two integral properties of the NDF are concerned (21). It is noteworthy that the number of conserved moments can be increased by distributing the born elements to more than two pivotal points as formulated by Alopaeus et al. (23).

Despite the competitive advantages of the fixed-pivot approach over previously developed approaches (24), Kumar & Ramkrishna (21) illustrated that the fixed-pivot approach overpredicts the NDF, particularly in the case of aggregation/coalescence. They stated that the overprediction issue arises due to the fixed pivotal points and proposed a new approach based on moving pivotal points. This method involves the solution for the number density (or a property of the NDF) at moving pivotal points, the location of which is governed by a differential equation. The locations of pivotal points change in such a way as to ensure preservation of the targeted properties. In another attempt to improve the predictions, a new technique was developed, called the cell-averaging technique, which assigns the born elements to the pivotal points on the basis of the average value of their internal coordinates (25). Numerical tests showed that the cell-averaging technique improves the results considerably (25). More details on this technique can be found elsewhere (25).

Concerning the continuous change of the internal coordinate, the third term on the left-hand side of Equation 7 can be written as

$$\int_{\xi_i}^{\xi_{i+1}} \partial_\xi (Gn)\, \mathrm{d}\xi = (Gn)|_{\xi_{i+1}} - (Gn)|_{\xi_i}, \qquad 10.$$

and it can be interpreted as the net flux of elements to/from the interval I_i, which is equal to the difference between the fluxes at the bounds of I_i. However, the NDF at the bounds of intervals is not known and must be approximated by interpolating the values at two neighboring pivotal points. The upwind scheme is the simplest interpolation approach. Consider a generic bound ξ_i at which the number density $n(\xi_i)$ is needed. If the rate of continuous process at the bound $G(\xi_i)$ is positive, then $n(\xi_i) = N_{i-1}$; otherwise $n(\xi_i) = N_i$. The upwind scheme is first order, and therefore it suffers from numerical diffusion (2). Numerical diffusion can be avoided by integration over the characteristic curves (26), but this method is not suited for being incorporated in CFD codes. A more viable alternative is employing high-order schemes (27–29), which, however, do not guarantee the positivity of the N_i (26). To overcome this issue, numerous methods have been proposed (1, 26).

Last, class or sectional methods can be extended to bi- and multivariate PBEs (30, 31). However, these extensions are not covered here as they are currently not compatible with CFD implementations because of their exceedingly large computational cost (16, 32, 33).

3.2. Method of Moments

The previous section mentioned several difficulties in tracking the evolution of the NDF through the direct solution of the PBE, which mainly arise due to the discretization of the internal coordinate space. In a pioneering work, Hulburt & Katz (34) argued that the NDF contains too much information for many engineering applications and proposed an approximate system of description that tracks the evolution of moments of the NDF instead of the NDF itself. In the most general form, the moments of the NDF are defined as

$$m_{k_1,k_2,\ldots,k_d,k_{d+1},k_{d+2},k_{d+3}}(t,\mathbf{x}) = \langle \xi_1^{k_1}\xi_2^{k_2}\ldots\xi_d^{k_d}u_1^{k_{d+1}}u_2^{k_{d+2}}u_3^{k_{d+3}}\rangle$$
$$= \int_{\Omega_{\boldsymbol{\xi}}}\int_{\Omega_{\mathbf{u}}} \xi_1^{k_1}\xi_2^{k_2}\ldots\xi_d^{k_d}u_1^{k_{d+1}}u_2^{k_{d+2}}u_3^{k_{d+3}}\, f(t,\mathbf{x},\boldsymbol{\xi},\mathbf{u})\,\mathrm{d}\boldsymbol{\xi}\,\mathrm{d}\mathbf{u}, \qquad 11.$$

where $\mathbf{k} = (k_1, k_2, \ldots, k_d, k_{d+1}, k_{d+2}, k_{d+3})$ is the exponent vector. Each element of $\mathbf{k}$ is the order of the moment with respect to the corresponding internal coordinate or velocity component. The moments offer two key advantages that make the method of moments (MOM) attractive. First, the moments are functions of only time and space, i.e., they are Eulerian fields, and therefore an approach based on the moments is perfectly compatible with the solution methods readily available in CFD codes. The second advantage is that the low-order moments are related to some macroscopic properties of the disperse phase, which are physically meaningful and generally measurable. It is noteworthy that, in many applications, the ultimate aim of solving the PBE is to predict these macroscopic properties of the disperse phase.

A simplified example helps to elaborate on the subject without loss of generality. Let the internal coordinates be comprised of the mass of the elements $\xi = M$ and the velocity. Then, the MOM involves the solution of a number of transport equations written in terms of the moments of the NDF. The moments $\langle \xi^0 u_1^0 u_2^0 u_3^0\rangle$, $\langle \xi^1 u_1^0 u_2^0 u_3^0\rangle$, and $\langle \xi^0 u_1^1 u_2^0 u_3^0\rangle$, $\langle \xi^0 u_1^0 u_2^1 u_3^0\rangle$, and $\langle \xi^0 u_1^0 u_2^0 u_3^1\rangle$ exemplify the importance of low-order moments, since they represent respectively the total particle number density, the average particle mass density, and the three components of the total particle momentum density.

The transport equation for a generic moment, $\langle \xi^{k_1} u_1^{k_2} u_2^{k_3} u_3^{k_4}\rangle$, is derived by multiplying the GPBE, Equation 3, with the function $g(\xi, \mathbf{u}) = \xi^{k_1} u_1^{k_2} u_2^{k_3} u_3^{k_4}$, and by integrating over the internal coordinate phase space:

$$\partial_t\left(\int_{\mathbb{R}^+}\mathrm{d}\xi\int_{\mathbb{R}^3} gf\,\mathrm{d}\mathbf{u}\right) + \partial_{\mathbf{x}}\cdot\left(\int_{\mathbb{R}^+}\mathrm{d}\xi\int_{\mathbb{R}^3}\mathbf{u}gf\,\mathrm{d}\mathbf{u}\right)$$
$$+\int_{\mathbb{R}^+}\mathrm{d}\xi\int_{\mathbb{R}^3} g\,\partial_\xi(Gf)\,\mathrm{d}\mathbf{u} + \int_{\mathbb{R}^+}\mathrm{d}\xi\int_{\mathbb{R}^3} g\,\partial_{\mathbf{u}}\cdot(\mathbf{A}f)\,\mathrm{d}\mathbf{u} = \int_{\mathbb{R}^+}\mathrm{d}\xi\int_{\mathbb{R}^3} g\mathcal{S}\,\mathrm{d}\mathbf{u}. \qquad 12.$$

The first term is the derivative of the moment with respect to time, $\partial_t\langle \xi^{k_1} u_1^{k_2} u_2^{k_3} u_3^{k_4}\rangle$. The second term is the moment transport in the physical space, which appears as the spatial derivative of a higher-order moment,

$$\partial_{\mathbf{x}}\cdot\left(\int_{\mathbb{R}^+}\mathrm{d}\xi\int_{\mathbb{R}^3}\mathbf{u}gf\,\mathrm{d}\mathbf{u}\right) = \partial_{x_1}\langle \xi^{k_1} u_1^{k_2+1} u_2^{k_3} u_3^{k_4}\rangle + \partial_{x_2}\langle \xi^{k_1} u_1^{k_2} u_2^{k_3+1} u_3^{k_4}\rangle$$
$$+\partial_{x_3}\langle \xi^{k_1} u_1^{k_2} u_2^{k_3} u_3^{k_4+1}\rangle, \qquad 13.$$

giving rise to the closure problem described below. The third term on the left-hand side of Equation 12 can be simplified further by integration by part (2):

$$\int_{\mathbb{R}^+} \mathrm{d}\xi \int_{\mathbb{R}^3} g\, \partial_\xi (Gf)\, \mathrm{d}\mathbf{u} = -\int_{\mathbb{R}^3} (gGf)|_{\xi=0}\, \mathrm{d}\mathbf{u} - \int_{\mathbb{R}^+} \mathrm{d}\xi \int_{\mathbb{R}^3} \partial_\xi (g)\, Gf\, \mathrm{d}\mathbf{u}. \qquad 14.$$

The first term on the right-hand side takes into account the appearance/disappearance of the disperse phase elements at the origin, which may be nonzero depending on the sign of G, i.e., if $g(\xi)$ is not zero and negative at the origin (2, 35). Likewise, the integration by part simplifies the fourth term on the left-hand side of Equation 12:

$$\int_{\mathbb{R}^+} \mathrm{d}\xi \int_{\mathbb{R}^3} g\, \partial_{\mathbf{u}} \cdot (\mathbf{A}f)\, \mathrm{d}\mathbf{u} = -\int_{\mathbb{R}^+} \mathrm{d}\xi \int_{\mathbb{R}^3} \mathbf{A}f \cdot \partial_{\mathbf{u}}(g)\, \mathrm{d}\mathbf{u}. \qquad 15.$$

The moment transport equations, i.e., Equation 12, are not in closed form, except in a few simple cases (2). One reason is that a set of transport equations written for a number of moments may contain terms which depend on higher-order moments. The addition of new moment transport equations for the higher-order moments would not solve the problem because the new equations give rise to new higher-order moments. However, the higher-order moments can be readily calculated if the NDF is known. In general, the knowledge of the NDF is also needed to calculate the source term and transport terms in the space of internal coordinates and velocity (see Equation 12). This is the main issue raised by the MOM and is known as the closure problem. Several methods have been developed to close the moment transport equations, such as interpolative closures (36), reconstruction of the NDF with an assumed functional form (37–39), and approximating the NDF using a quadrature formula (40–42). The reader can find more details on developed closures elsewhere (2, 43). This work focuses on the closures based on the quadrature formula, known as quadrature-based moment methods (QBMMs), which have more general applicability than other proposed closures.

3.3. Quadrature-Based Moment Methods

In QBMMs, the NDF is approximated with an N-node quadrature formula, i.e., a summation of N weighted kernel density functions, each centered on a node/abscissa of a Gaussian quadrature approximation. The most commonly employed kernel density function is the Dirac delta function. The idea originated with McGraw (40), who employed an N-node Gaussian quadrature to approximate the integrals in the moment transport equations for the solution of a univariate PBE and named the approach quadrature method of moments (QMOM). The algorithm calculates the N abscissas and N weights of the quadrature from the $2N$ transported moments. Marchisio & Fox (42) developed a similar method, named direct quadrature method of moments (DQMOM), by which the quadrature approximation is transported in space and time such that the moments evolve according to the proper transport equations. In the following sections, both approaches are explained in detail. Moreover, the extension of the QMOM to bi- and multivariate PBEs (i.e., the conditional quadrature method of moments, CQMOM) is also discussed. Last, we introduce the extended quadrature method of moments (EQMOM), which is useful in applications that require a continuous reconstruction of the NDF.

3.3.1. Quadrature method of moments. McGraw (40) proposed that the unclosed integrals of the moment transport equations can be approximated by employing an N-node Gaussian quadrature formula. It is equivalent to assuming the following functional form to approximate the NDF

(for a univariate problem):

$$n(t,\mathbf{x},\xi) \approx \sum_{p=1}^{N} w_p(t,\mathbf{x})\,\delta[\xi - \xi_p(t,\mathbf{x})], \tag{16.}$$

where $w_p(t,\mathbf{x})$ and $\xi_p(t,\mathbf{x})$ are the weight and abscissa of the node p. In the above expression, δ denotes the Dirac delta function. The moment of order k of the approximated NDF can be expressed as follows:

$$m_k = \int_{\mathbb{R}^+} \xi^k n(\xi)\,\mathrm{d}\xi \approx \sum_{p=1}^{N} w_p\,\xi_p^k, \tag{17.}$$

where m_k is an alternative notation for $\langle \xi^k \rangle$. The above relationship implies that knowledge about the first $2N$ moments enables us to determine the N weights and N abscissas of the quadrature approximation in Equation 16 by solving the following set of nonlinear equations:

$$m_0 = \sum_{p=1}^{N} w_p\,, \quad m_1 = \sum_{p=1}^{N} w_p\,\xi_p^1\,, \quad \ldots \quad m_{2N-1} = \sum_{p=1}^{N} w_p\,\xi_p^{2N-1}. \tag{18.}$$

The above set of nonlinear equations is usually solved by employing well-conditioned recursive inversion algorithms such as the product-difference (PD) algorithm (44) and the Wheeler algorithm (45). The latter has the advantage of being applicable to distributions with zero mean value, i.e., $m_1 = 0$, in contrast to the PD algorithm (2). It is noteworthy that the weights and abscissas obtained from the solution of Equation 18 reproduce exactly the moments up to order $2N-1$.

The QMOM employs an N-node quadrature approximation to solve the transport equations for a set of moments of a PBE. The QMOM procedure can be explained by writing the transport equation of a generic moment of order k derived from the PBE (Equation 1):

$$\partial_t(m_k) + \partial_{\mathbf{x}} \cdot (\mathbf{U}_{\mathrm{d},k} m_k) = \delta_{k,0}\, G(0)\, n(0) + k \int_{\mathbb{R}^+} \xi^{k-1}\, G n\,\mathrm{d}\xi + \int_{\mathbb{R}^+} \xi^k \mathcal{S}\,\mathrm{d}\xi, \tag{19.}$$

where $\delta_{k,0}$ is the Kronecker delta and $\mathbf{U}_{\mathrm{d},k}$ denotes the transport velocity of the k-order moment defined by

$$\mathbf{U}_{\mathrm{d},k} = \frac{1}{m_k} \int_{\mathbb{R}^+} \xi^k \mathbf{U}_{\mathrm{d}}(\xi)\, n\,\mathrm{d}\xi. \tag{20.}$$

The first term on the right-hand side of Equation 19 appears only in the transport equation of the zeroth-order moment. This term is particularly challenging in the case of negative G, or in other words when the disperse phase elements are shrinking and disappearing. More detailed discussion on the subject can be found in References 6 and 46. In the latter reference, a method is suggested to reconstruct a continuous NDF by using the maximum entropy maximization, which enables the evaluation of the NDF at the origin (i.e., $\xi = 0$). In addition, a robust and efficient quadrature-based method was developed by Yuan and coworkers (47) to reconstruct a continuous NDF (see Section 3.3.4). The second term on the right-hand side of Equation 19 can be approximated using the N-node Gaussian quadrature formula:

$$k \int_{\mathbb{R}^+} \xi^{k-1}\, G(\xi) n(\xi)\,\mathrm{d}\xi \approx k \sum_{p=1}^{N} w_p \xi_p^{k-1} G(\xi_p). \tag{21.}$$

The source term in the case of aggregation/coalescence and breakage is approximated likewise (assuming that ξ is a conserved property such as mass or volume of elements) (2):

$$\int_{\mathbb{R}^+} \xi^k \mathcal{S}\, \mathrm{d}\xi \approx \frac{1}{2} \sum_{p=1}^{N} w_p \sum_{q=1}^{N} (\xi_p + \xi_q)^k a(\xi_p, \xi_q)\, w_q - \sum_{p=1}^{N} \xi_p^k\, a(\xi_p, \xi_q)\, w_p$$
$$+ \sum_{p=1}^{N} \left(\int_{\mathbb{R}^+} \xi^k \beta(\xi|\xi_p)\, \mathrm{d}\xi \right) b(\xi_p)\, w_p - \sum_{p=1}^{N} \xi_p^k\, b(\xi_p)\, w_p. \qquad 22.$$

The weights and abscissas of the quadrature formula in Equations 21 and 22 are determined by inverting the first $2N$ moments. Therefore, it is necessary to track the evolution of the first $2N$ moments by solving the corresponding transport equations. At each time step, the quadrature formula is determined by means of an inversion algorithm, which uses the $2N$ transported moments available from the previous time step or the initial conditions. It is noteworthy that the inversion algorithm fails if the moments are not realizable, i.e., the moment set is not inside the moment space (see the sidebar titled Moment Space). The realizability issue is mainly due to the numerical methods that deal with the discretized moment transport equations, which are not the same as the exact equations. This fact necessitates employing numerical methods that are designed to prevent the realizability issue (48–52).

In general, a quadrature formula with more nodes yields a more accurate approximation of integrals in the moment transport equations and an approximation of higher quality for the NDF. However, a quadrature with more nodes means more moments to be tracked, hence the need for more computational resources. In addition, the recursive algorithms for the calculation of the weights and abscissas become less stable as the number of nodes increases, and convergence gets difficult for typically $N > 10$ (2). However, Marchisio and colleagues (41, 53) showed that satisfactory predictions can be achieved by employing a quadrature approximation with $2 \leq N \leq 4$ for simple aggregation and breakage problems. Moreover, QMOM predictions have acceptably small overall error not only for the tracked moments but also for higher-order moments (41).

Concerning bi- and multivariate PBEs, the main challenge is the determination of the weights and (multidimensional) abscissas of the quadrature from the mixed moments, since the PD and Wheeler algorithms are applicable only to univariate quadratures. The next section focuses on the extension of the QMOM to such cases by using conditional moments.

MOMENT SPACE

Any number density function $n(\xi)$ defined on a support Ω_ξ can be associated with a positive measure (μ) such that $\mathrm{d}\mu = n(\xi)\, \mathrm{d}\xi$. One can consider all the possible measures defined on the same support Ω_ξ, which together form a space of measures denoted by $\mathcal{P}$. Then, each possible measure $\mu \in \mathcal{P}$ determines a possible vector of k moments (from order 0 to k): $\mathbf{m}_k = (m_0, m_1, \ldots, m_k)$. Eventually, the kth-order moment space ($\mathcal{M}_k$) on the support Ω_ξ is defined as the space formed by all the possible $\mathbf{m}_k$, each corresponding to a $\mu \in \mathcal{P}$, or mathematically: $\mathcal{M}_k = \{\mathbf{m}_k = \int_{\Omega_\xi} (\xi^0, \xi^1, \ldots, \xi^k)\, \mathrm{d}\mu | \mu \in \mathcal{P}\}$. A set of moments $(m_0, m_1, \ldots, m_k)$ should belong to the moment space $\mathcal{M}_k$ to be realizable; otherwise, no positive measure can be found with such a set of moments. The characterization of the moment space $\mathcal{M}_k$ for three common supports $\Omega_\xi = (-\infty, \infty)$, $\Omega_\xi = (0, \infty)$, and $\Omega_\xi = (0, 1)$ is found in Reference 87.

3.3.2. Conditional quadrature method of moments. This section deals with the application of the QBMM to the solution of bi- and multivariate PBEs. Let the NDF be defined over the space (Ω_ξ) of d internal coordinates, $\boldsymbol{\xi} = (\xi_1, \xi_2, \ldots, \xi_d)$. Then, the NDF can be approximated with the following functional form:

$$n(t, \mathbf{x}, \boldsymbol{\xi}) \approx \sum_{p=1}^{N} w_p(t, \mathbf{x})\, \boldsymbol{\delta}[\boldsymbol{\xi} - \boldsymbol{\xi}_p(t, \mathbf{x})], \quad \boldsymbol{\delta}[\boldsymbol{\xi} - \boldsymbol{\xi}_p(t, \mathbf{x})] = \prod_{\alpha=1}^{d} \delta[\xi_\alpha - \xi_{\alpha;p}(t, \mathbf{x})], \tag{23.}$$

where $w_p(t, \mathbf{x})$ is the weight of the node p with abscissas $\boldsymbol{\xi}_p = (\xi_{1;p}, \xi_{2;p}, \ldots, \xi_{d;p})$ located in the joint space of the internal coordinates. The reader should bear in mind that the above quadrature is not a Gaussian quadrature. Moreover, univariate inversion methods such as PD or Wheeler algorithms are not applicable to multivariate density functions. The moments of the above approximation can be expressed as follows:

$$\langle \xi_1^{k_1} \xi_2^{k_2} \ldots \xi_d^{k_d} \rangle = m_{k_1,k_2,\ldots,k_d} = \sum_{p=1}^{N} w_p \prod_{\alpha=1}^{d} \xi_{\alpha;p}^{k_\alpha}. \tag{24.}$$

The closure problem can be overcome by determining the quadrature approximation of order N, defined by N weights and N d-dimensional abscissas/nodes. The weights and abscissas of the quadrature nodes can be found by using a set of $N(d + 1)$ moments. The inversion approach is desired to have some main properties of univariate inversion algorithms (2).

First, it should be noniterative—otherwise its application to practical CFD simulations will be computationally expensive. Second, it should construct a mathematically and physically meaningful quadrature approximation—in other words, abscissas should be located in the support of the internal coordinates and weights should be nonnegative. Last, the weights and abscissas obtained from the moments of an N-point density function should represent exactly the same N-point density function. Several methods have been developed to determine the high-dimensional quadrature points, such as the brute-force algorithm (54), the tensor-product algorithm (55–58), and the CQMOM (59, 60), just to cite the most popular. Only the last method is discussed here, since it is generally more stable and accurate.

For the sake of brevity, the explanation focuses on the bivariate NDF. The extension of the following procedure to more than two internal coordinates can be found elsewhere (2). In addition, the application of the CQMOM to the kinetic equations, i.e., three velocity components as the internal coordinates, is discussed by Yuan & Fox (60). In the CQMOM, the NDF is approximated by the following functional form:

$$n(t, \mathbf{x}, \boldsymbol{\xi}) \approx \sum_{p_1=1}^{N_1} \sum_{p_2=1}^{N_2} w_{p_1}(t, \mathbf{x})\, w_{p_2,p_1}(t, \mathbf{x})\, \delta[\xi_1 - \xi_{1;p_1}(t, \mathbf{x})]\, \delta[\xi_2 - \xi_{2;p_2,p_1}(t, \mathbf{x})], \tag{25.}$$

where w_{p_1} and $\xi_{1;p_1}$ are the weights and abscissas calculated from the pure moments with respect to the first internal coordinate (ξ_1) by using a univariate inversion algorithm. Instead, w_{p_2,p_1} and $\xi_{2;p_2,p_1}$ are the conditional weights and abscissas to be obtained by conditioning the second internal coordinate (ξ_2) on each abscissa of the first one ($\xi_{1;p_1}$). The calculation of the conditional weights and abscissas exploits the relationship between the mixed moments and the conditional NDF ($n_{2|1}$). First, the conditional NDF is defined by

$$n_{2|1}(\xi_2|\xi_1) = \frac{n(\xi_1, \xi_2)}{n_1(\xi_1)}, \tag{26.}$$

where $n_1(\xi_1) = \int_{\Omega_{\xi_2}} n(\xi_1, \xi_2)\, \mathrm{d}\xi_2$ is the marginal NDF of ξ_1. The moments of $n_1(\xi_1)$ are the same as the pure moments of $n(\xi_1, \xi_2)$ with respect to ξ_1 and therefore can be expressed in terms of w_{p_1} and $\xi_{1;p_1}$. Then, the mixed moments can be written as follows:

$$\begin{aligned} m_{k_1,k_2} &= \int_{\Omega_{\xi_1}} \xi_1^{k_1} n_1(\xi_1)\, \mathrm{d}\xi_1 \int_{\Omega_{\xi_2}} \xi_2^{k_2} n_{2|1}(\xi_2|\xi_1)\, \mathrm{d}\xi_2 \\ &= \sum_{p_1=1}^{N_1} w_{p_1} \xi_{1;p_1}^{k_1} \int_{\Omega_{\xi_2}} \xi_2^{k_2} n_{2|1}(\xi_2|\xi_{1;p_1}^{k_1})\, \mathrm{d}\xi_2 = \sum_{p_1=1}^{N_1} w_{p_1} \xi_{1;p_1}^{k_1} \langle \xi_2^{k_2} \rangle (\xi_{1;p_1}), \end{aligned} \tag{27.}$$

where $\langle \xi_2^{k_2} \rangle (\xi_{1;p_1})$ denotes the conditional moments. Using the above relationship, the $N_1(2N_2 - 1)$ conditional moments can be obtained from the solution of the linear systems of the following form written for $k_2 = 0, \ldots, 2N_2 - 1$:

$$\begin{bmatrix} 1 & \cdots & 1 \\ \xi_{1;1} & \cdots & \xi_{1;N_1} \\ \vdots & \ddots & \vdots \\ \xi_{1;1}^{N_1-1} & \cdots & \xi_{1;N_1}^{N_1-1} \end{bmatrix} \begin{bmatrix} w_1 & & \\ & w_2 & \\ & & \ddots \\ & & w_{N_1} \end{bmatrix} \begin{bmatrix} \langle \xi_2^{k_2} \rangle (\xi_{1;1}) \\ \langle \xi_2^{k_2} \rangle (\xi_{1;2}) \\ \vdots \\ \langle \xi_2^{k_2} \rangle (\xi_{1;N_1}) \end{bmatrix} = \begin{bmatrix} m_{0,k_2} \\ m_{1,k_2} \\ \vdots \\ m_{N_1-1,k_2} \end{bmatrix}. \tag{28.}$$

The above linear system of equations, known as the Vandermonde linear system, is nonsingular as long as the abscissas $\xi_{1;p1}$ are distinct. The reader is referred to Reference 61 for an efficient algorithm to solve the linear systems of the Vandermonde form. Finally, for each $\xi_{1;p1}$, a univariate inversion algorithm is applied to the corresponding set of conditional moments to find the corresponding conditional weights (w_{p_2,p_1}) and abscissas ($\xi_{2;p_2,p_1}$). Although the pure moments can be kept realizable by employing an appropriate numerical scheme, the realizability of the conditional moments is not guaranteed. In this case, the realizability issue can be overcome by applying the 1-D adaptive quadrature technique proposed by Yuan & Fox (60). With this technique, the maximum number of conditional moments belonging to the moment space is determined, and consequently, the number of nodes for the second internal coordinate (at each $\xi_{1;p1}$) is adjusted accordingly.

One should pay attention to the selected order of internal coordinates' conditioning as it changes the set of controlled moments (i.e., moments used in the reconstruction of the NDF). Nevertheless, all the moments controlled in the CQMOM belong to the optimal moment set; see Section 3.3.3 for the definition and importance of such a set.

3.3.3. Direct quadrature method of moments. The DQMOM was first introduced by Marchisio & Fox (42) to avoid the need for an inversion algorithm, particularly in the case of bi-/multivariate problems. Although the inversion of moments in bi-/multivariate problems was later overcome by the CQMOM, the DQMOM has received considerable attention from the scientific community. Furthermore, the DQMOM can be applied to univariate problems.

In contrast to the QMOM and CQMOM, the DQMOM employs transport equations written in terms of the weights w_p and weighted abscissas $\varsigma_{\alpha;p} = w_p \xi_{\alpha;p}$. Therefore, there is no need to employ an inversion algorithm except for the initialization of the weights and abscissas according to the initial conditions of the moments. Let the NDF be defined over the space of two internal

coordinates and governed by the following bivariate PBE:

$$\partial_t n + \partial_{\mathbf{x}} \cdot (\langle \mathbf{u}|\xi_1, \xi_2\rangle n) + \partial_{\xi_1}(G_1 n) + \partial_{\xi_2}(G_2 n) = \int \mathcal{S}\, \mathrm{d}\mathbf{u}. \tag{29.}$$

The DQMOM approximates the NDF with the functional form in Equation 23. Then, the following transport equations can be written for the weights and weighted abscissas (42):

$$\begin{aligned} \partial_t w_p + \partial_{\mathbf{x}} \cdot (\langle \mathbf{u}\rangle_p w_p) &= s_p^w, \\ \partial_t(\varsigma_{1;p}) + \partial_{\mathbf{x}} \cdot (\langle \mathbf{u}\rangle_p \varsigma_{1;p}) &= s_{1,p}^{\varsigma}, \\ \partial_t(\varsigma_{2;p}) + \partial_{\mathbf{x}} \cdot (\langle \mathbf{u}\rangle_p \varsigma_{2;p}) &= s_{2,p}^{\varsigma}, \end{aligned} \tag{30.}$$

where $\langle \mathbf{u}\rangle_p = \langle \mathbf{u}|\xi_{1,p}, \xi_{2,p}\rangle$ denotes the velocity of the quadrature node p, and s_p^w, $s_{1,p}^{\varsigma}$ and $s_{1,p}^{\varsigma}$ are the source terms of the transport equations to be determined. The unknown source terms can be found by first replacing the NDF in Equation 29 with the functional form in Equation 23 specialized for a bivariate problem and then applying the moment transformation of a generic order $\mathbf{k} = (k_1, k_2)$ (42):

$$\sum_{p=1}^{N}(1 - k_1 - k_2)\xi_{1,p}^{k_1}\xi_{2,p}^{k_2}s_p^w - \sum_{p=1}^{N} k_1 \xi_{1,p}^{k_1-1}\xi_{2,p}^{k_2}s_{1,p}^{\varsigma} + \sum_{p=1}^{N} k_2 \xi_{1,p}^{k_1}\xi_{2,p}^{k_2-1}s_{2,p}^{\varsigma} = \bar{h}_{k_1,k_2}, \tag{31.}$$

where $\bar{h}_{k_1,k_2}$ takes into account the change of the moment due to the continuous and discontinuous events and therefore is problem dependent. A system of $3N$ linear equations (equal to the number of unknowns) can be formed by writing Equation 31 for $3N$ moments of different order. The solution of the linear system can be expressed in the matrix form $\mathbf{s} = \mathcal{A}^{-1}\mathbf{h}$, where $\mathbf{s} = [s_1^w \ldots s_N^w\, s_{1,1}^{\varsigma} \ldots s_{1,N}^{\varsigma}\, s_{2,1}^{\varsigma} \ldots s_{2,N}^{\varsigma}]^T$ and $\mathcal{A}$ is the coefficient matrix. The matrix $\mathcal{A}$ should be nonsingular and therefore requires some considerations. First, the abscissas must remain distinct in order to prevent singularity. Thus, using too many nodes is not recommended, since the probability of two nodes approaching each other increases with the addition of more nodes (2). Another important point is the choice of the moment set, which Fox (62) discusses in detail. Fox established a methodology to choose a set of moments, called the optimal moment set, that results in a nonsingular coefficient matrix $\mathcal{A}$. Eventually, Fox reported the optimal moment sets for problems with $1 \leq d \leq 3$. The concept was developed by using $N = r^d$ nodes for $r \in \mathbb{Z}_{>0}$, which treats all the internal coordinates equally. It is noteworthy that other choices for the moment set might work as well, which are valid but not optimal. However, one should try to use a moment set that covers the important moments, i.e., those with physical significance, and that includes enough mixed moments to avoid losing the correlation between the internal coordinates. For more details, the reader is referred to the discussion of choosing the moment set in Reference 2.

3.3.4. Extended quadrature method of moments. The previous QBMMs approximate the NDF with an N-point discontinuous distribution, i.e., a summation of N weighted Dirac delta functions. However, some applications require a continuous reconstructed NDF to correctly model the phenomena involved, e.g., evaporating sprays (46). Yuan et al. (47) suggested a method, called the extended quadrature method of moments (EQMOM), which employs a parametric continuous kernel density function (KDF) instead of the Dirac delta function:

$$n(t, \mathbf{x}, \xi) \approx \sum_{p=1}^{N} w_p(t, \mathbf{x})\, \delta_\sigma[\xi; \xi_p(t, \mathbf{x})], \tag{32.}$$

where $\delta_\sigma(\xi;\xi_p)$ is a chosen KDF, which depends on the parameter σ. The weights and abscissas associated with the KDF are denoted by w_p and ξ_p. The determination of the parameter σ requires that one additional moment should be tracked, in comparison to the $2N$ moments tracked in the QMOM. The KDF is required to reduce smoothly to the Dirac delta function in the limit of $\sigma \to 0$, meaning that the quadrature can be reconstructed from the first $2N$ moments when $\sigma = 0$. The choice of the KDF is problem dependent, i.e., the support of the KDF should be consistent with the support of the internal coordinate. Common KDFs are Gaussian distribution with infinite support $(-\infty, \infty)$, gamma and log-normal distributions with semi-infinite positive support $[0, \infty)$, and beta distribution with finite support [0, 1]. Moreover, it is practically important that the selected KDF can be defined in terms of the weight function $w(\theta)$ for a known family of orthogonal polynomials. In the following, the algorithm for the calculation of the weights and abscissas of the quadrature approximation as well as the parameter σ are explained for a univariate NDF with semi-infinite positive support. The application of the EQMOM to problems with infinite or finite supports is similar and can be found elsewhere (2, 47). In addition, the reader is referred to Reference 2 for the extension of the EQMOM to multivariate problems.

As mentioned, a suitable choice of KDF for problems with support of $[0, \infty)$ is the gamma distribution. Then, the NDF is approximated by the following summation of N weighted parameterized gamma distributions:

$$n(\xi) \approx \sum_{p=1}^{N} w_p \frac{\xi^{\lambda_p - 1} e^{-\xi/\sigma}}{\Gamma(\lambda_p)\sigma^{\lambda_p}} \quad \text{and} \quad \lambda_p(t, \mathbf{x}) = \frac{\xi_p}{\sigma}, \tag{33.}$$

where Γ is the gamma function. The moments of the NDF can be expressed as

$$m_k(t, \mathbf{x}) = \sum_{p=1}^{N} w_p \frac{\Gamma(\lambda_p + k)}{\Gamma(\lambda_p)} \sigma^k = \sum_{p=1}^{N} w_p \xi_p^k + \sum_{p=1}^{N} w_p P_{k-1}(\xi_p, \sigma), \tag{34.}$$

where $P_{k-1}(\xi_p, \sigma)$ is a homogeneous polynomial of order $k - 1$ with respect to ξ_p and σ. The summation $\sum_{p=1}^{N} w_p \xi_p^k$ is indeed the kth-order moment of the quadrature in the limit $\sigma = 0$, and here is denoted by m_k^*. Equation 34 can be written for the first $2N + 1$ moments to calculate the weights and abscissas as well as the parameter σ of the quadrature. An important observation is that the right-hand side of Equation 34 can be rewritten in terms of only m_k^* and σ. Subsequently, the two sets of moments $\mathbf{m} = (m_0, m_1, \ldots, m_{2N})$ and $\mathbf{m}^* = (m_0^*, m_1^*, \ldots, m_{2N}^*)$ can be related through the matrix form $\mathbf{m} = \mathbf{B}(\sigma)\mathbf{m}^*$. The matrix $\mathbf{B}(\sigma)$ is a lower-triangular matrix, which allows us to calculate the moment m_k^* from the moments $(m_0, m_1, \ldots, m_k)$ for a given value of σ. Eventually, the following iterative approach can be used to determine the quadrature approximation (47):

1. Guess the parameter σ and calculate the first $2N$ moments $(m_0^*, m_1^*, \ldots, m_{2N-1}^*)$ using $\mathbf{m}^* = \mathbf{B}^{-1}(\sigma)\mathbf{m}$
2. Find the weights w_p and abscissas ξ_p from the moments $(m_0^*, m_1^*, \ldots, m_{2N-1}^*)$ by employing the adaptive quadrature algorithm
3. Use the weights and abscissas to calculate $m_{2N}^* = \sum_{p=1}^{N} w_p \xi_p^{2N}$
4. Calculate the scalar function $J(\sigma) = m_{2N} - m_{2N}^* - \sum_{p=1}^{N} w_p P_{2N-1}(\xi_p, \sigma)$
5. Guess a new σ until the convergence $J(\sigma) = 0$ is achieved for the smallest σ

In the above approach, the adaptive quadrature algorithm allows us to cope with the nonrealizable set of moments. Once the quadrature is determined, it can be used to close the terms appearing in the moment transport equations, i.e., Equation 32. For this purpose, a general

integral of the NDF is considered:

$$\int_{\Omega_\xi} g(\xi)n(\xi)\,\mathrm{d}\xi = \sum_{p=1}^{N} w_p \int_{\Omega_\xi} g(\xi)\delta_\sigma(\xi;\xi_p)\,\mathrm{d}\xi = \sum_{p=1}^{N}\sum_{q=1}^{N'} w_p w_q^{(p)}\, g(\xi_q^{(p)}), \qquad 35.$$

where $g(\xi)$ is a generic function of the internal coordinate. In Equation 35, the integral of the KDF $\delta_\sigma(\xi;\xi_p)$ is approximated by a quadrature formula, for which the weights $w_q^{(p)}$ and abscissas $\xi_q^{(p)}$ can be calculated from the recursion coefficients that are known in advance. Moreover, the number of nodes of the second quadrature (N') does not depend on N and can be increased independently to improve the accuracy.

3.4. Selection of the Solution Method

A key factor in selection of the solution method is the number of internal coordinates. For univariate problems, the CM and QMOM are regarded as the first candidates. The CM is more suitable for simulation of systems in which the NDF can be measured directly. In contrast, the QMOM provides information about some (usually measurable) integral properties of the NDF. From the computational point of view, the QMOM is normally less demanding than the CM. In fact, achieving a reasonable accuracy by the CM generally requires a large number of intervals/classes, which is computationally expensive, particularly when disperse phase elements span a wide region of the phase space (41). Therefore, the QMOM is the preferred method for the CFD simulation of spatially heterogeneous systems, specifically those of large scale (5). Furthermore, the CM should use high-order schemes when the system under study involves continuous events, in particular if the number of intervals cannot be increased sufficiently. However, employing high-order schemes usually leads to instabilities. In contrast, QBMMs handle continuous events easily, if the growth rate is positive. In cases of negative growth rates, e.g., evaporation/dissolution, the EQMOM can be used to estimate the value of the NDF at the origin of the relevant internal coordinate. Moreover, the EQMOM should be generally used when the particulate processes of interest are highly localized in the phase space (63). In fact, with other QBMMs, some phenomena may be ignored if there is no node/abscissa in the region where they are active. Furthermore, the addition of nodes does not necessarily improve the situation, as the QMOM shows unpredictable behavior in response to the increase in the number of nodes, when highly localized phenomena are present (63). In such cases, the CM or EQMOM are more appropriate.

In the case of bi- and multivariate PBEs, QBMMs are generally the preferred methods. Both the DQMOM and CQMOM were developed to overcome the difficulties of moment inversion in bi- and multivariate problems. However, the CQMOM has some advantages over the DQMOM. Firstly, the equivalence between the DQMOM and QMOM/CQMOM is lost in pure hyperbolic PBEs (2), in contrast to spatially homogeneous systems. Moreover, the DQMOM is not valid for purely hyperbolic PBEs in the presence of (spatial or time) discontinuity in the weights and abscissas, because the transport equations in Equation 30 are derived on the assumption that the weights and abscissas are continuous functions of time and space (2). Another point is that the DQMOM does not guarantee the conservation of the moments except for the moments of order zero and one, and needs corrective terms to respect the conservation of the moments of higher order (2). Last, when a continuous NDF is needed, the CQMOM can be extended to use a KDF other than the Dirac delta function, i.e., the extended CQMOM (2).

4. IMPLEMENTATION IN COMPUTATIONAL FLUID DYNAMICS

Particle trajectory crossing (PTC): in dilute systems, particles of different velocity (regardless of their properties) can cross each other without collision

As mentioned above, the solution of the GPBE/PBE provides detailed information about the disperse phase, which can result in a more accurate solution. For instance, a more accurate estimation of the drag force can be obtained by using the instantaneous size distribution of the disperse phase elements instead of a fixed constant element size. At the same time, the solution of the GPBE/PBE requires knowledge of the flow fields. Therefore, it is necessary to adopt a suitable approach to couple CFD and the GPBE/PBE, as explained in the following section.

4.1. Monokinetic Models

Monokinetic models, e.g., the TFM and MFM, assume zero velocity dispersion around the mean velocity (or mean velocities) of elements located at the same spatial coordinates at a given time and characterized by the same internal coordinate values. This assumption is valid for elements with small Stokes numbers (below 1) (13). Within this context, the simplest approach assigns one velocity, $\mathbf{U}_d(t, \mathbf{x})$, to all elements of the disperse phase, which depends only on the spatial coordinates and time and not on the internal coordinates. The common methods for obtaining the velocity of the disperse phase, required to solve the PBE, include the MM and TFM (5, 32, 64–71), although the dusty gas approach (72) and the equilibrium Eulerian approach (13) can be used for sufficiently small elements (12). At the same time, the polydispersity of the elements can be described through the solution of the PBE, Equation 1, by using a suitable method described in the previous section. When the CM is used to solve the PBE, the coupling terms are evaluated using the properties of each class of disperse elements. In contrast, if we adopt the QMOM, the coupling terms are calculated by using either the average properties of the disperse elements, which are associated with the moments, or the quadrature nodes separately (16).

The assumption of identical element velocity can be relaxed partially by employing a multifluid approach, where the elements are grouped into several phases based on the value of an internal coordinate (usually size). When the CM is chosen to solve the PBE (3, 65, 73–75), each class is assumed to move with its own velocity. In the case of the QMOM or DQMOM (5, 8, 76, 77), each node of the quadrature moves with a unique velocity. The velocity of each class (or node in the case of the QMOM or DQMOM) is obtained either by solving a momentum balance equation written for the corresponding class (or node) or by adopting the MM (see Section 2.3).

The monokinetic assumption is not valid in the case of elements with large Stokes numbers, since large elements do not adapt quickly to the surrounding fluid velocity and therefore the effect of their initial conditions lasts for a long time (13). For instance, this assumption may lead to nonphysical predictions in dilute systems consisting of particles characterized by large Stokes numbers, where particle trajectory crossing (PTC) can occur (48, 57). A possible approach to describing such systems is adoption of a polykinetic model.

4.2. Polykinetic Models

It is necessary to include the element velocity as an internal coordinate, when dealing with disperse systems far from equilibrium or composed of elements characterized by very large Stokes numbers. In such cases, the evolution of the disperse phase in space and time is entirely governed by the GPBE, Equation 3, while the continuous phase is described by Equations 5 and 6. The interaction between the phases is taken into account through the exchange terms in the governing equations of both phases. The quadrature-based methods are preferred to solve the GPBE, since the application of the CM to this equation is not tractable. In this regard, the QMOM, DQMOM and specifically CQMOM are promising tools to solve the GPBE (2, 6, 48, 57–60).

When the disperse system is very dilute, the effect of the disperse phase on the flow field of the continuous phase can be assumed negligible (2, 78). Thus, one-way coupling suffices to describe the effect of the continuous phase on the evolution of the disperse phase elements. The flow fields of the continuous phase are predicted by the solution of the single-phase Navier-Stokes equations. At each time step, the governing equations of the continuous phase are solved to predict the flow fields of the continuous phase, which eventually will be used to estimate the closure relations in the GPBE. It is possible to advance the GPBE with several smaller time steps within each time step of the CFD solver, if the timescale of the phenomena affecting the elements is comparably smaller than the characteristic timescale of the continuous phase (78).

However, the effect of disperse elements on flow fields of the continuous phase becomes significant as the number density of elements increases. Thus, governing equations of the continuous phase should include exchange terms due to the presence of the disperse phase elements, e.g., Equations 5 and 6 (79, 80). Convergence issues may arise in the two-way coupling due to the explicit exchange terms included in the governing equations. For instance, the drag force generally depends on the relative velocity of the phases and, if handled explicitly, hinders convergence. The convergence rate can be improved by adopting the partial elimination algorithm (81). The application of the partial elimination algorithm to CFD-QMOM simulations is explained by Passalacqua and coworkers (78, 79).

High-resolution (HR) total variation diminishing (TVD) schemes: interpolation schemes that employ a flux limiter to prevent oscillations in the solution of hyperbolic problems (83, 84)

4.3. Numerical Issues of Quadrature-Based Moment Methods

Efficient numerical methods for solving the PBE must provide sufficiently accurate solutions as well as ensure the stability of the simulation. A major reason for simulation instabilities is the appearance of nonphysical solutions during the simulation, i.e., the realizability issue associated with the QBMM. The realizability issue appears mostly when standard high-order schemes are employed for the independent advection of the moments (82). These schemes aim mainly at achieving high-order and oscillation-free solutions for transported variables. However, the moments are linked variables that belong to the moment space; therefore, a selected numerical scheme must additionally ensure that the moment space is preserved. Unfortunately, only first-order schemes, e.g., the upwind scheme, are guaranteed to yield realizable moment sets provided that the Courant–Friedrichs–Lewy (CFL) condition is satisfied (48). It is noteworthy that the CFL condition generally serves as the criterion for the stability of the CFD simulations. The first-order schemes, despite being very stable, generally produce diffused solutions for computationally affordable grid sizes. Therefore, if high-order solutions are required, one must employ high-order schemes that are specifically designed to overcome the realizability issue.

In a pioneering work, Vikas and coworkers (49) proposed the quasi-high-order realizable scheme, which interpolates separately the weights and abscissas of the quadrature (instead of the moments) from the cell centers to the faces. In this approach, the quadrature weights on the faces are obtained with a high-resolution (HR) total variation diminishing (TVD) scheme, whereas the quadrature abscissas on the faces are obtained by using the first-order upwind scheme. With this technique, it is possible to avoid the realizability issue if a criterion for the time step is fulfilled (49). This approach works for the solution of both the PBE and GPBE. Moreover, it can be simply implemented in CFD codes, regardless of the spatial dimensionality and mesh type. Another notable approach preserves the moment space by advecting a sequence of positive variables, called ζ, which are connected to the moments (51). The application of the original version of this approach to arbitrary unstructured grids is not straightforward. Nevertheless, Passalacqua and coworkers (85) extended the applicability of this approach to unstructured meshes.

In addition to the realizability issue, the boundedness of the solution is another important numerical aspect because the low-order moments are associated with some average physical properties of the elements, which are bounded in nature (86). This aspect should be considered in the selection of the numerical solution method if a bounded solution for the moments is desired. For instance, Shiea and coworkers (52) observed oscillations in the solution for the advection of moments in a one-dimensional Riemann problem obtained by using a quasi-second-order realizable scheme. They argued that an oscillation-free solution for the moments is not necessarily guaranteed when the HR TVD schemes are not applied directly to the moments. Eventually, they suggested that it is possible to apply the HR TVD schemes directly to the moments without encountering the realizability issue by using an identical limiter (equal limiter) for all the transported moments (52). They additionally showed that the boundedness of the moments is guaranteed if the equal limiter is set to the smallest limiter among those calculated independently for the transported moments.

4.4. Computational Fluid Dynamics–Population Balance Equation Codes

Apart from the numerous in-house codes reported in the literature, there are several commercial and open-source CFD codes, which incorporate the PBE. **Table 1** summarizes some available CFD-PBE codes along with their main features.

5. SUCCESS STORIES

As mentioned before, the formulation of classical Eulerian-Eulerian CFD methods is not capable of fully addressing the polydispersity, i.e., the distribution of disperse elements, that is a feature of many multiphase systems and needs a joint CFD-PBE approach to be taken into account. Furthermore, even monodisperse or slightly polydisperse systems can take advantage of the CFD-PBE approach when the average elements' size (or other properties of interest) evolves under the effect

Table 1 Commercial and open-source computational fluid dynamics (CFD) codes with the implementation of population balance equations (PBEs)

CFD code	Governing equations	Solution methods	Notes
OpenFOAM[a]	Equation 1 Equation 3	CM QMOM[b] CQMOM[b] EQMOM[b]	Multifluid approach is available Possibility of solving several population balances Realizable advection schemes are implemented
Ansys Fluent	Equation 1	CM QMOM DQMOM	Multifluid approach is available
Ansys CFX	Equation 1	CM	Multifluid approach is available PBE is written in terms of mass-based NDF Continuous events and nucleation are not available
StarCCM	Equation 1	CM	Multifluid approach is available Adaptive discretization

[a]Open-source.
[b]Part of the OpenQBMM project (**https://www.openqbmm.org**).
Abbreviations: CM, class method; CQMOM, conditional quadrature method of moments; DQMOM, direct quadrature method of moments; EQMOM, extended quadrature method of moments; NDF, number density function; QMOM, quadrature method of moments.

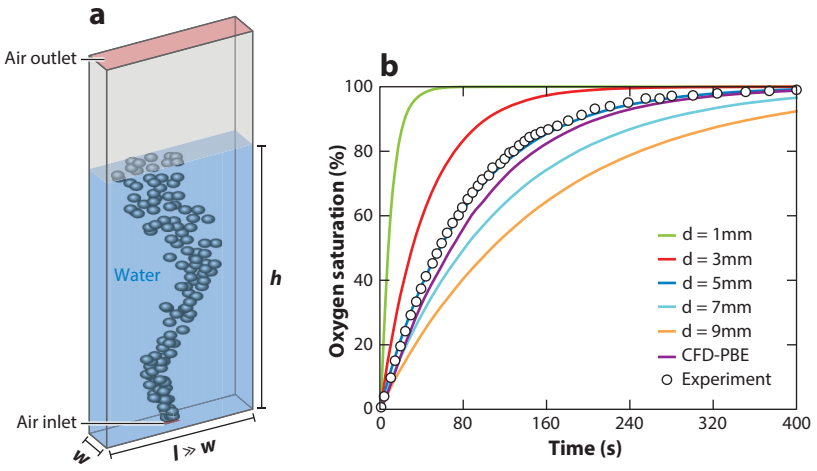

Figure 4

(*a*) Schematic representation of a pseudo–two-dimensional bubble column, in which the oxygen is absorbed from the air bubbles into the water. (*b*) The predictions for the average concentration of oxygen in water versus time obtained by the fixed bubble size CFD simulations and the CFD–PBE simulation are compared with the experimental data taken from Reference 120. Abbreviations: CFD, computational fluid dynamics; PBE, population balance equation.

of the aggregation/coalescence, breakage, and growth/shrinkage. For instance, **Figure 4** depicts a pseudo–two-dimensional bubble column in which the oxygen is dissolved from the disperse phase (air bubbles) into the continuous phase (water). The absorption process continues until the dissolved oxygen reaches saturation. The generated bubbles belong to a narrow size distribution and therefore the system can be assumed to be monodisperse. An important key factor for the design of such mass-transfer processes is the bubble size. In fact, the mass-transfer rate depends on the interfacial area that, in turn, depends on the bubble size. In addition, the bubble size determines the terminal velocity of the bubbles and consequently their residence time in the system. **Figure 4** illustrates the effect of the bubble size on the dynamics of the oxygen absorption in the depicted bubble column. Each colored curve represents the prediction by a monodisperse CFD simulation, i.e., with a fixed bubble size. The purple curve, instead, is the prediction by the CFD-PBE approach. The comparison of the predictions with the experiments (hollow circles) shows that the proper setting of the bubble size is necessary to reproduce the experimental data. However, the PBE can estimate this important property of the bubbles when it is not known in advance. Moreover, **Figure 4** implies that simulations with a fixed bubble size (linked with the classical CFD method) can misrepresent the dynamics of the system if the bubble size distribu-tion is too wide, i.e., the system is polydisperse. In this case, the PBE is an appropriate tool to address the polydispersity of bubbles.

The literature offers countless applications of the PBE coupled with the CFD, which include a variety of disperse systems. Gas–liquid systems, e.g., bubble columns, bubbly flows, and stirred tanks, have been studied extensively by the CFD-PBE approach, mostly with a univariate NDF in terms of the bubble size (67, 74, 88–93). In addition, several works solved for PBEs written in terms of multivariate NDFs, e.g., joint mass–velocity (94, 95) and joint size–concentration (32, 69, 96) NDFs. Other relevant works involve the application of the PBE in the CFD simulation of boiling flows with heat and mass transfer (97–99). Another popular category of CFD-PBE applications concerns gas–solid systems, including fluidized beds (5, 100–102), riser reactors

(103), and soot formation in flames (66, 104, 105). Furthermore, the CFD-PBE was successfully applied to simulate dilute gas–particle flows, for which the assumption of equilibrium may hardly apply, and therefore, the classical Eulerian-Eulerian approach fails to capture nonequilibrium phenomena, e.g., PTC. Other notable applications of the CFD-PBE include the simulation of liquid–liquid dispersions (71, 106–112), precipitation of particles (59, 113–115), evaporating sprays (7, 116), bioreactors (117, 118), and porous media (119).

It is noteworthy that there exist numerous other applications of the PBE in the literature, in which the PBE is employed to follow the evolution of (mostly homogeneous) disperse systems without being coupled with the CFD. In fact, disperse systems evolve under the simultaneous effects of different phenomena, e.g., mixing, aggregation/coalescence, breakage, and reaction. In general, when the timescales associated with the involved phenomena are comparable, the corresponding governing equations should be coupled and solved together. However, if the rate of mixing is much faster than that of the other phenomena, its effect can be decoupled from the solution of the PBE. An example helps to illustrate this point. Let us consider the liquid–liquid contactor, shown in **Figure 5**, that operates under turbulent conditions. The disperse phase consists of octanol droplets that are kept immersed in the continuous phase (water) by the rotating impeller. The size distribution of the droplets is determined by the coalescence and breakup, which depend on the turbulence generated by the impeller's rotation. The intensity of rotation determines also the mixing of the entire system. If the timescale of mixing is much smaller than the one associated with the coalescence and breakup of droplets, the assumption of spatial homogeneity holds. In this case, the PBE (Equation 1), with no convective term, can be used to describe the disperse system. This framework is known as the zero-dimensional model. As the volume fraction of the disperse phase increases, the rate of coalescence and breakup of droplets increases—in other words, the timescale associated with the combination of the coalescence and breakup decreases (see **Figure 5**). When the timescales of the mixing and coalescence/breakup become comparable,

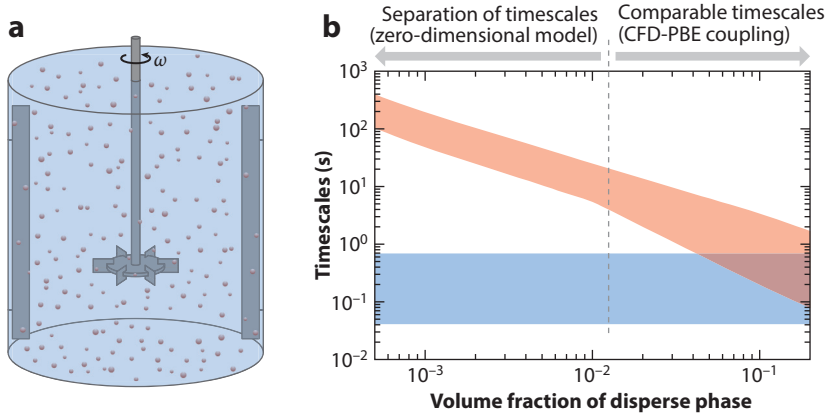

Figure 5

(*a*) Schematic representation of an agitated liquid–liquid contactor with water as the continuous phase and octanol as the disperse phase (droplets). (*b*) Comparison between the timescale of mixing (*blue shaded area*) and the one associated with the combination of coalescence and breakup (*red shaded area*) (109). When the disperse system is dilute, it can be assumed homogeneous, since the mixing timescale is much smaller than the one associated with the combination of the coalescence and breakup. In this case, it is possible to adopt a zero-dimensional model to describe the disperse system. However, the denser the disperse system, the faster the rate of the coalescence and breakup, hence the necessity of coupling the computational fluid dynamics (CFD) and population balance equation (PBE).

the two-way coupling of the CFD and PBE is generally required to correctly describe the behavior of the disperse system (110).

6. CONCLUDING REMARKS

We have introduced some main numerical methods for the solution of the PBE coupled with the CFD and highlighted the advantages of the CFD-PBE method for the simulation of disperse systems. In particular, it is currently the only tractable method, from the computational point of view, for the description of disperse systems consisting of a large number of disperse elements, usually seen in industrial-scale multiphase systems. Moreover, as the available computational power increases and the associated cost decreases, the CFD-PBE offers a fast predictive tool for the simulation of disperse systems in comparison to other detailed but computationally expensive alternatives. However, the successful application of this approach relies on the adopted numerical method and on the employed constitutive relations to describe the involved physical phenomena. Therefore, both aspects deserve attention in order to improve the predictability and generalize the applicability of the CFD-PBE approach. We hope that this review helps researchers of diverse communities to exploit the introduced methods in their field of interest and additionally motivates further research on the development of new techniques, which take into account various aspects such as robustness, stability, realizability of moments, order of accuracy, solution boundedness, and applicability to unstructured grids.

SUMMARY POINTS

1. We describe the governing equations for the Eulerian CFD-PBE simulation of disperse multiphase systems.
2. We explain the common methods for the solution of the PBE and present a guideline to select a suitable one.
3. When the Stokes number of elements is sufficiently small (<1), the monokinetic assumption is valid and the velocity of the disperse phase is predicted by a multiphase CFD solver. Otherwise, the GPBE governs the evolution of the distribution of the elements over the space of the internal properties, including the velocity.
4. In the QBMM, the realizability issue is the main cause of simulation instability and can be addressed by adopting the numerical schemes mentioned in this review. In addition, particular attention should be paid to the boundedness of the solution of the moment transport equations, when realizable schemes are employed.
5. Some discussed approaches for the simulation of disperse multiphase systems are accessible through several available commercial and open-source CFD-PBE codes; we report the leading ones.

FUTURE ISSUES

1. Despite the existing advances, the development of more robust numerical methods which increase simultaneously the accuracy and the stability of simulations, e.g., realizable numerical schemes, continues to be an interesting subject.

2. It is fruitful to develop efficient CFD-PBE codes or contribute to improve the existing ones, particularly the open-source codes as in the OpenQBMM project (**https://www.openqbmm.org**). These codes expand the application of the PBE to vast relevant subjects spanning broad scientific and industrial communities, which ultimately lead to rapid advances in different aspects of PBEs.

DISCLOSURE STATEMENT

The authors are not aware of any affiliations, memberships, funding, or financial holdings that might be perceived as affecting the objectivity of this review.

LITERATURE CITED

1. Ramkrishna D. 2000. *Population Balances: Theory and Applications to Particulate Systems in Engineering*. San Diego: Academic. 1st ed.
2. Marchisio DL, Fox RO. 2013. *Computational Models for Polydisperse Particulate and Multiphase Systems*. Cambridge Sser. Chem. Eng. Cambridge, UK: Cambridge Univ. Press
3. Laurent F, Massot M. 2001. Multi-fluid modelling of laminar polydisperse spray flames: origin, assumptions and comparison of sectional and sampling methods. *Combust. Theory Model.* 5:537–72
4. Laurent F, Massot M, Villedieu P. 2004. Eulerian multi-fluid modeling for the numerical simulation of coalescence in polydisperse dense liquid sprays. *J. Comput. Phys.* 194:505–43
5. Fan R, Marchisio DL, Fox RO. 2004. Application of the direct quadrature method of moments to polydisperse gas-solid fluidized beds. *Powder Technol.* 139:7–20
6. Fox RO, Laurent F, Massot M. 2008. Numerical simulation of spray coalescence in an Eulerian framework: direct quadrature method of moments and multi-fluid method. *J. Comput. Phys.* 227:3058–88
7. De Chaisemartin S, Fréret L, Kah D, Laurent F, Fox R, et al. 2009. Eulerian models for turbulent spray combustion with polydispersity and droplet crossing. *C. R. Mécan.* 337:438–48
8. Mazzei L, Marchisio DL, Lettieri P. 2012. New quadrature-based moment method for the mixing of inert polydisperse fluidized powders in commercial CFD codes. *AIChE J.* 58:3054–69
9. Drew DA. 2001. A turbulent dispersion model for particles or bubbles. *J. Eng. Math.* 41:259–74
10. Zaichik L, Simonin O, Alipchenkov V. 2009. An Eulerian approach for large eddy simulation of particle transport in turbulent flows. *J. Turbulence* 10:1–21
11. Fox RO. 2012. Large-eddy-simulation tools for multiphase flows. *Annu. Rev. Fluid Mech.* 44:47–76
12. Balachandar S, Eaton JK. 2010. Turbulent dispersed multiphase flow. *Annu. Rev. Fluid Mech.* 42:111–33
13. Ferry J, Balachandar S. 2001. A fast Eulerian method for disperse two-phase flow. *Int. J. Multiphase Flow* 27:1199–226
14. Manninen M, Taivassalo V, Kallio S. 1996. *On the Mixture Model for Multiphase Flow*. VTT Publication 288. Espoo: Tech. Res. Cent. Finland (VTT)
15. Sanyal J, Vásquez S, Roy S, Dudukovic M. 1999. Numerical simulation of gas–liquid dynamics in cylindrical bubble column reactors. *Chem. Eng. Sci.* 54:5071–83
16. Buffo A, Marchisio DL. 2014. Modeling and simulation of turbulent polydisperse gas-liquid systems via the generalized population balance equation. *Rev. Chem. Eng.* 30:73–126
17. Kataoka I, Serizawa A. 1989. Basic equations of turbulence in gas-liquid two-phase flow. *Int. J. Multiphase Flow* 15:843–55
18. Lopez de Bertodano MA, Saif AA. 1997. Modified $k - \varepsilon$ model for two-phase turbulent jets. *Nuclear Eng. Des.* 172:187–96
19. Peirano E, Leckner B. 1998. Fundamentals of turbulent gas-solid flows applied to circulating fluidized bed combustion. *Progress Energy Combust. Sci.* 24:259–96

20. Troshko A, Hassan Y. 2001. A two-equation turbulence model of turbulent bubbly flows. *Int. J. Multiphase Flow* 27:1965–2000
21. Kumar S, Ramkrishna D. 1996. On the solution of population balance equations by discretization—I. A fixed pivot technique. *Chem. Eng. Sci.* 51:1311–32
22. Gelbard F, Tambour Y, Seinfeld JH. 1980. Sectional representations for simulating aerosol dynamics. *J. Colloid Interface Sci.* 76:541–56
23. Alopaeus V, Laakkonen M, Aittamaa J. 2006. Solution of population balances with breakage and agglomeration by high-order moment-conserving method of classes. *Chem. Eng. Sci.* 61:6732–52
24. Vanni M. 2000. Approximate population balance equations for aggregation-breakage processes. *J. Colloid Interface Sci.* 221:143–60
25. Kumar J, Peglow M, Warnecke G, Heinrich S, Mörl L. 2006. Improved accuracy and convergence of discretized population balance for aggregation: the cell average technique. *Chem. Eng. Sci.* 61:3327–42
26. Kumar S, Ramkrishna D. 1997. On the solution of population balance equations by discretization—III. Nucleation, growth and aggregation of particles. *Chem. Eng. Sci.* 52:4659–79
27. Marchal P, David R, Klein J, Villermaux J. 1988. Crystallization and precipitation engineering—I. An efficient method for solving population balance in crystallization with agglomeration. *Chem. Eng. Sci.* 43:59–67
28. David R, Villermaux J, Marchal P, Klein JP. 1991. Crystallization and precipitation engineering—IV. Kinetic model of adipic acid crystallization. *Chem. Eng. Sci.* 46:1129–36
29. Hounslow M, Ryall R, Marshall V. 1988. A discretized population balance for nucleation, growth, and aggregation. *AIChE J.* 34:1821–32
30. Kumar J, Peglow M, Warnecke G, Heinrich S. 2008. The cell average technique for solving multidimensional aggregation population balance equations. *Comput. Chem. Eng.* 32:1810–30
31. Buffo A, Alopaeus V. 2016. Solution of bivariate population balance equations with high-order moment-conserving method of classes. *Comput. Chem. Eng.* 87:111–24
32. Buffo A, Vanni M, Marchisio DL, Fox RO. 2013. Multivariate quadrature-based moments methods for turbulent polydisperse gas-liquid systems. *Int. J. Multiphase Flow* 50:41–57
33. Buffo A, Marchisio DL, Vanni M, Renze P. 2013. Simulation of polydisperse multiphase systems using population balances and example application to bubbly flows. *Chem. Eng. Res. Des.* 91:1859–75
34. Hulburt HM, Katz S. 1964. Some problems in particle technology: a statistical mechanical formulation. *Chem. Eng. Sci.* 19:555–74
35. Fox RO. 2007. Introduction and fundamentals of modeling approaches for polydisperse multiphase flows. In *Multiphase Reacting Flows: Modelling and Simulation. CISM International Centre for Mechanical Sciences*, ed. DL Marchisio, RO Fox, Vol. 492, pp. 1–40. Vienna: Springer
36. Frenklach M. 2002. Method of moments with interpolative closure. *Chem. Eng. Sci.* 57:2229–39
37. Lee K. 1983. Change of particle size distribution during Brownian coagulation. *J. Colloid Interface Sci.* 92:315–25
38. Kruis FE, Kusters KA, Pratsinis SE, Scarlett B. 1993. A simple model for the evolution of the characteristics of aggregate particles undergoing coagulation and sintering. *Aerosol Sci. Technol.* 19:514–26
39. Strumendo M, Arastoopour H. 2008. Solution of PBE by MOM in finite size domains. *Chem. Eng. Sci.* 63:2624–40
40. McGraw R. 1997. Description of aerosol dynamics by the quadrature method of moments. *Aerosol Sci. Technol.* 27:255–65
41. Marchisio DL, Vigil RD, Fox RO. 2003. Quadrature method of moments for aggregation-breakage processes. *J. Colloid Interface Sci.* 258:322–34
42. Marchisio DL, Fox RO. 2005. Solution of population balance equations using the direct quadrature method of moments. *J. Aerosol Sci.* 36:43–73
43. Diemer R, Olson J. 2002. A moment methodology for coagulation and breakage problems: Part 2—moment models and distribution reconstruction. *Chem. Eng. Sci.* 57:2211–28
44. Gordon RG. 1968. Error bounds in equilibrium statistical mechanics. *J. Math. Phys.* 9:655–63
45. Wheeler JC. 1974. Modified moments and Gaussian quadratures. *Rocky Mt. J. Math.* 4:287–96

46. Massot M, Laurent F, Kah D, De Chaisemartin S. 2010. A robust moment method for evaluation of the disappearance rate of evaporating sprays. *SIAM J. Appl. Math.* 70:3203–34
47. Yuan C, Laurent F, Fox RO. 2012. An extended quadrature method of moments for population balance equations. *J. Aerosol Sci.* 51:1–23
48. Desjardins O, Fox RO, Villedieu P. 2008. A quadrature-based moment method for dilute fluid-particle flows. *J. Comput. Phys.* 227:2514–39
49. Vikas V, Wang ZJ, Passalacqua A, Fox RO. 2011. Realizable high-order finite-volume schemes for quadrature-based moment methods. *J. Comput. Phys.* 230:5328–52
50. Kah D, Laurent F, Massot M, Jay S. 2012. A high order moment method simulating evaporation and advection of a polydisperse liquid spray. *J. Comput. Phys.* 231:394–422
51. Laurent F, Nguyen TT. 2017. Realizable second-order finite-volume schemes for the advection of moment sets of the particle size distribution. *J. Comput. Phys.* 337:309–38
52. Shiea M, Buffo A, Vanni M, Marchisio D. 2018. A novel finite-volume TVD scheme to overcome non-realizability problem in quadrature-based moment methods. *J. Comput. Phys.* 409:109337
53. Marchisio DL, Soos M, Sefcik J, Morbidelli M. 2006. Role of turbulent shear rate distribution in aggregation and breakage processes. *AIChE J.* 52:158–73
54. Wright DL Jr., McGraw R, Rosner DE. 2001. Bivariate extension of the quadrature method of moments for modeling simultaneous coagulation and sintering of particle populations. *J. Colloid Interface Sci.* 236:242–51
55. Yoon C, McGraw R. 2004. Representation of generally mixed multivariate aerosols by the quadrature method of moments: I. Statistical foundation. *J. Aerosol Sci.* 35:561–76
56. Yoon C, McGraw R. 2004. Representation of generally mixed multivariate aerosols by the quadrature method of moments: II. Aerosol dynamics. *J. Aerosol Sci.* 35:577–98
57. Fox RO. 2008. A quadrature-based third-order moment method for dilute gas-particle flows. *J. Comput. Phys.* 227:6313–50
58. Fox RO. 2009. Higher-order quadrature-based moment methods for kinetic equations. *J. Comput. Phys.* 228:7771–91
59. Cheng JC, Fox RO. 2010. Kinetic modeling of nanoprecipitation using CFD coupled with a population balance. *Ind. Eng. Chem. Res.* 49:10651–62
60. Yuan C, Fox RO. 2011. Conditional quadrature method of moments for kinetic equations. *J. Comput. Phys.* 230:8216–46
61. Press WH, Teukolsky SA, Vetterling WT, Flannery BP. 2007. *Numerical Recipes: The Art of Scientific Computing*. New York: Cambridge Univ. Press. 3rd ed.
62. Fox RO. 2009. Optimal moment sets for multivariate direct quadrature method of moments. *Ind. Eng. Chem. Res.* 48:9686–96
63. Grosch R, Briesen H, Marquardt W, Wulkow M. 2007. Generalization and numerical investigation of QMOM. *AIChE J.* 53:207–27
64. Sanyal J, Marchisio DL, Fox RO, Dhanasekharan K. 2005. On the comparison between population balance models for CFD simulation of bubble columns. *Ind. Eng. Chem. Res.* 44:5063–72
65. Chen P, Duduković M, Sanyal J. 2005. Three-dimensional simulation of bubble column flows with bubble coalescence and breakup. *AIChE J.* 51:696–712
66. Zucca A, Marchisio DL, Barresi AA, Fox RO. 2006. Implementation of the population balance equation in CFD codes for modelling soot formation in turbulent flames. *Chem. Eng. Sci.* 61:87–95
67. Bannari R, Kerdouss F, Selma B, Bannari A, Proulx P. 2008. Three-dimensional mathematical modeling of dispersed two-phase flow using class method of population balance in bubble columns. *Comput. Chem. Eng.* 32:3224–37
68. Petitti M, Nasuti A, Marchisio DL, Vanni M, Baldi G, et al. 2010. Bubble size distribution modeling in stirred gas-liquid reactors with QMOM augmented by a new correction algorithm. *AIChE J.* 56:36–53
69. Buffo A, Vanni M, Marchisio DL. 2012. Multidimensional population balance model for the simulation of turbulent gas-liquid systems in stirred tank reactors. *Chem. Eng. Sci.* 70:31–44
70. Buffo A, Vanni M, Marchisio D. 2017. Simulation of a reacting gas–liquid bubbly flow with CFD and PBM: validation with experiments. *Appl. Math. Model.* 44:43–60

71. Li D, Gao Z, Buffo A, Podgorska W, Marchisio DL. 2017. Droplet breakage and coalescence in liquid–liquid dispersions: comparison of different kernels with EQMOM and QMOM. *AIChE J.* 63:2293–311
72. Marble FE. 1970. Dynamics of dusty gases. *Annu. Rev. Fluid Mech.* 2:397–446
73. Krepper E, Lucas D, Frank T, Prasser HM, Zwart PJ. 2008. The inhomogeneous MUSIG model for the simulation of polydispersed flows. *Nuclear Eng. Des.* 238:1690–702
74. Bhole M, Joshi J, Ramkrishna D. 2008. CFD simulation of bubble columns incorporating population balance modeling. *Chem. Eng. Sci.* 63:2267–82
75. Selma B, Bannari R, Proulx P. 2010. Simulation of bubbly flows: comparison between direct quadrature method of moments (DQMOM) and method of classes (CM). *Chem. Eng. Sci.* 65:1925–41
76. Silva LFLR, Lage PLC. 2011. Development and implementation of a polydispersed multiphase flow model in OpenFOAM. *Comput. Chem. Eng.* 35:2653–66
77. Icardi M, Ronco G, Marchisio DL, Labois M. 2014. Efficient simulation of gas–liquid pipe flows using a generalized population balance equation coupled with the algebraic slip model. *Appl. Math. Model.* 38:4277–90
78. Passalacqua A, Vedula P, Fox RO. 2011. Quadrature-based moment methods for polydisperse gas-solids flows. In *Computational Gas-Solids Flows and Reacting Systems: Theory, Methods and Practice*, ed. S Pannala, M Syamlal, TJ O'Brien, pp. 221–44. Hershey, PA: IGI Global
79. Passalacqua A, Fox R, Garg R, Subramaniam S. 2010. A fully coupled quadrature-based moment method for dilute to moderately dilute fluid–particle flows. *Chem. Eng. Sci.* 65:2267–83
80. Fox RO, Vedula P. 2009. Quadrature-based moment model for moderately dense polydisperse gas-particle flows. *Ind. Eng. Chem. Res.* 49:5174–87
81. Spalding D. 1980. Numerical computation of multi-phase fluid flow and heat transfer. In *Recent Advances in Numerical Methods in Fluids*, ed. C Taylor, K Morgan, pp. 139–67. Swansea, UK: Pineridge
82. Wright DL Jr. 2007. Numerical advection of moments of the particle size distribution in Eulerian models. *J. Aerosol Sci.* 38:352–69
83. Harten A. 1983. High resolution schemes for hyperbolic conservation laws. *J. Comput. Phys.* 49:357–93
84. LeVeque RJ. 2002. *Finite Volume Methods for Hyperbolic Problems*. Cambridge, UK: Cambridge Univ. Press. 1st ed.
85. Passalacqua A, Laurent F, Fox RO. 2020. A second-order realizable scheme for moment advection on unstructured grids. *Comput. Phys. Commun.* 248:106993
86. Buffo A, Vanni M, Marchisio DL. 2016. On the implementation of moment transport equations in OpenFOAM: boundedness and realizability. *Int. J. Multiphase Flow* 85:223–35
87. Pigou M, Morchain J, Fede P, Penet MI, Laronze G. 2018. New developments of the extended quadrature method of moments to solve population balance equations. *J. Comput. Phys.* 365:243–68
88. Venneker BC, Derksen JJ, Van den Akker HE. 2002. Population balance modeling of aerated stirred vessels based on CFD. *AIChE J.* 48:673–85
89. Wang T, Wang J. 2007. Numerical simulations of gas–liquid mass transfer in bubble columns with a CFD-PBM coupled model. *Chem. Eng. Sci.* 62:7107–18
90. Petitti M, Nasuti A, Marchisio DL, Vanni M, Baldi G, et al. 2010. Bubble size distribution modeling in stirred gas–liquid reactors with QMOM augmented by a new correction algorithm. *AIChE J.* 56:36–53
91. Peña-Monferrer C, Passalacqua A, Chiva S, Muñoz-Cobo JL. 2016. CFD modelling and validation of upward bubbly flow in an adiabatic vertical pipe using the quadrature method of moments. *Nucl. Eng. Des.* 301:320–32
92. Renze P, Buffo A, Marchisio DL, Vanni M. 2014. Simulation of coalescence, breakup, and mass transfer in polydisperse multiphase flows. *Chem. Ing. Tech.* 86:1088–98
93. Gemello L, Plais C, Augier F, Marchisio DL. 2019. Population balance modelling of bubble columns under the heterogeneous flow regime. *Chem. Eng. J.* 372:590–604
94. Yuan C, Kong B, Passalacqua A, Fox RO. 2014. An extended quadrature-based mass-velocity moment model for polydisperse bubbly flows. *Can. J. Chem. Eng.* 92:2053–66
95. Heylmun JC, Kong B, Passalacqua A, Fox RO. 2019. A quadrature-based moment method for polydisperse bubbly flows. *Comput. Phys. Commun.* 244:187–204

96. Petitti M, Vanni M, Marchisio DL, Buffo A, Podenzani F. 2013. Simulation of coalescence, break-up and mass transfer in a gas-liquid stirred tank with CQMOM. *Chem. Eng. J.* 228:1182–94
97. Yeoh G, Tu J. 2004. Population balance modelling for bubbly flows with heat and mass transfer. *Chem. Eng. Sci.* 59:3125–39
98. Cheung SC, Yeoh G, Tu J. 2008. Population balance modeling of bubbly flows considering the hydrodynamics and thermomechanical processes. *AIChE J.* 54:1689–710
99. Krepper E, Rzehak R, Lifante C, Frank T. 2013. CFD for subcooled flow boiling: coupling wall boiling and population balance models. *Nucl. Eng. Des.* 255:330–46
100. Mazzei L, Marchisio DL, Lettieri P. 2010. Direct quadrature method of moments for the mixing of inert polydisperse fluidized powders and the role of numerical diffusion. *Ind. Eng. Chem. Res.* 49:5141–52
101. Chen XZ, Luo ZH, Yan WC, Lu YH, Ng IS. 2011. Three-dimensional CFD-PBM coupled model of the temperature fields in fluidized-bed polymerization reactors. *AIChE J.* 57:3351–66
102. Yan WC, Luo ZH, Lu YH, Chen XD. 2012. A CFD-PBM-PMLM integrated model for the gas–solid flow fields in fluidized bed polymerization reactors. *AIChE J.* 58:1717–32
103. Li J, Luo ZH, Lan XY, Xu CM, Gao JS. 2013. Numerical simulation of the turbulent gas–solid flow and reaction in a polydisperse FCC riser reactor. *Powder Technol.* 237:569–80
104. Zucca A, Marchisio DL, Vanni M, Barresi AA. 2007. Validation of bivariate DQMOM for nanoparticle processes simulation. *AIChE J.* 53:918–931
105. Bisetti F, Blanquart G, Mueller ME, Pitsch H. 2012. On the formation and early evolution of soot in turbulent nonpremixed flames. *Combust. Flame* 159:317–35
106. Attarakih MM, Bart HJ, Faqir NM. 2006. Numerical solution of the bivariate population balance equation for the interacting hydrodynamics and mass transfer in liquid–liquid extraction columns. *Chem. Eng. Sci.* 61:113–23
107. Schmidt SA, Simon M, Attarakih MM, Lagar L, Bart HJ. 2006. Droplet population balance modelling hydrodynamics and mass transfer. *Chem. Eng. Sci.* 61:246–56
108. Drumm C, Attarakih MM, Bart HJ. 2009. Coupling of CFD with DPBM for an RDC extractor. *Chem. Eng. Sci.* 64:721–32
109. Roudsari SF, Turcotte G, Dhib R, Ein-Mozaffari F. 2012. CFD modeling of the mixing of water in oil emulsions. *Comput. Chem. Eng.* 45:124–36
110. Buffo A, De Bona J, Vanni M, Marchisio DL. 2016. Simplified volume-averaged models for liquid–liquid dispersions: correct derivation and comparison with other approaches. *Chem. Eng. Sci.* 153:382–93
111. De Bona J, Buffo A, Vanni M, Marchisio DL. 2016. Limitations of simple mass transfer models in polydisperse liquid–liquid dispersions. *Chem. Eng. J.* 296:112–21
112. Gao Z, Li D, Buffo A, Podgórska W, Marchisio DL. 2016. Simulation of droplet breakage in turbulent liquid–liquid dispersions with CFD-PBM: comparison of breakage kernels. *Chem. Eng. Sci.* 142:277–88
113. Gavi E, Rivautella L, Marchisio D, Vanni M, Barresi A, Baldi G. 2007. CFD modelling of nano-particle precipitation in confined impinging jet reactors. *Chem. Eng. Res. Des.* 85:735–44
114. Di Pasquale N, Marchisio D, Barresi A. 2012. Model validation for precipitation in solvent-displacement processes. *Chem. Eng. Sci.* 84:671–83
115. Cheng J, Yang C, Mao ZS. 2012. CFD-PBE simulation of premixed continuous precipitation incorporating nucleation, growth and aggregation in a stirred tank with multi-class method. *Chem. Eng. Sci.* 68:469–80
116. Kah D, Laurent F, Fréret L, De Chaisemartin S, Fox RO, et al. 2010. Eulerian quadrature-based moment models for dilute polydisperse evaporating sprays. *Flow Turbul. Combust.* 85:649–76
117. Morchain J, Gabelle JC, Cockx A. 2014. A coupled population balance model and CFD approach for the simulation of mixing issues in lab-scale and industrial bioreactors. *AIChE J.* 60:27–40
118. Wodołażski A. 2020. Co-simulation of CFD-multiphase population balance coupled model aeration of sludge flocs in stirrer tank bioreactor. *Int. J. Multiph. Flow* 123:103162
119. Boccardo G, Sethi R, Marchisio DL. 2019. Fine and ultrafine particle deposition in packed-bed catalytic reactors. *Chem. Eng. Sci.* 198:290–304
120. Cachaza EM, Díaz ME, Montes FJ, Galán MA. 2009. Simultaneous computational fluid dynamics (CFD) simulation of the hydrodynamics and mass transfer in a partially aerated bubble column. *Ind. Eng. Chem. Res*. 48:8685–96